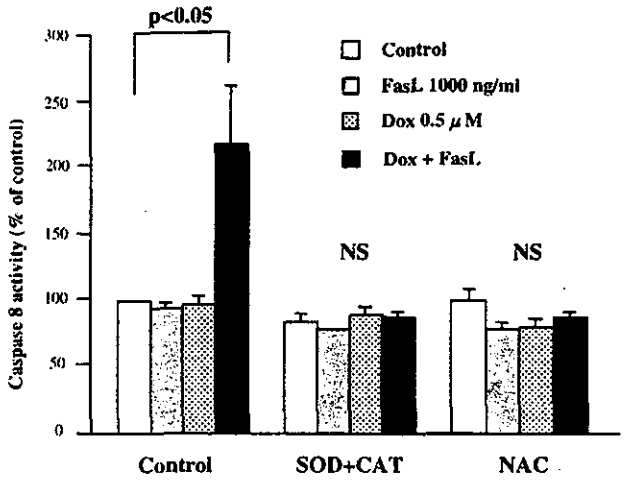

Fig. 4. Enzymatic activities of caspase-8 in cardiac myocytes. Caspase 8 activity was dramatically enhanced after both treatments of recombinant Fas ligand (FasL: 1 μg/ml) and doxorubicin (Dox: 0.5 μM). *N*-acetylcysteine (NAC) and the combination of superoxide dismutase (SOD) and catalase (CAT) abolished the enhancement of caspase-8 activity after both treatments of FasL and doxorubicin. Concentrations were as follows: SOD 500 U/ml, CAT 500 U/ml, and NAC 50 μmol/l. Results are expressed as mean±S.E.M. of three separate experiments.

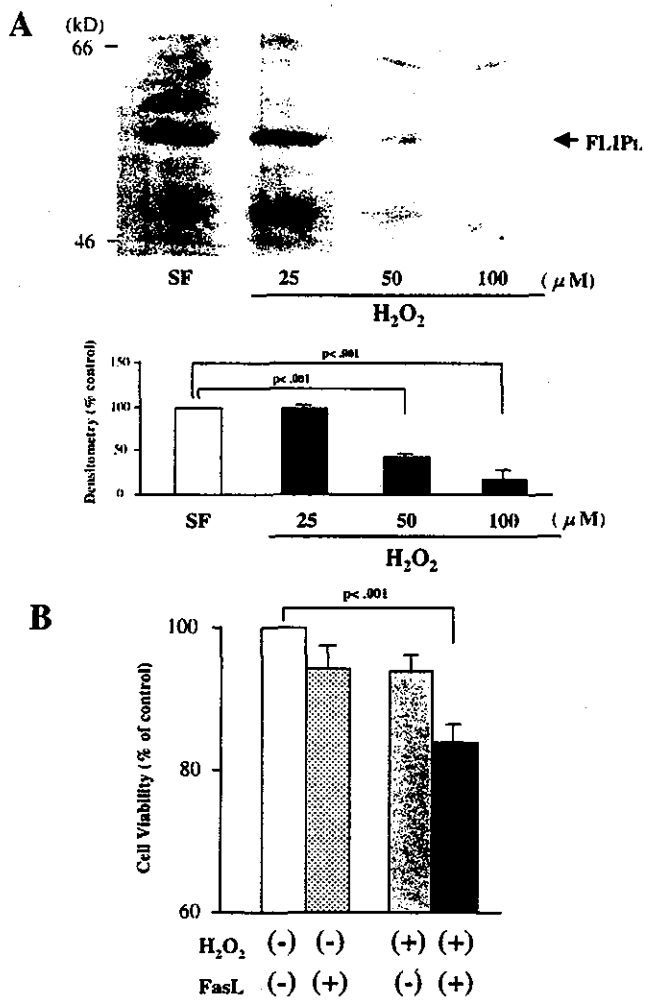

Fig. 5. Hydrogen peroxide (H_2O_2) down-regulated the expression of $FLIP_L$ and sensitized cardiac myocytes to Fas. (A) The expression of $FLIP_L$ (55 kDa) was determined by Western blot analysis in cardiomyocytes incubated with various doses of hydrogen peroxide for 24 h. $FLIP_L$ expression was quantified by densitometry. (B) Cardiac myocytes were incubated with human recombinant Fas ligand (FasL: 1 μg/ml) for 12 h after 12 h treatment with H_2O_2 (50 μmol/l). Cell viability was determined by MTT assay. $^*P<0.01$ vs. untreated cells. Results are expressed as mean±S.E.M. of three separate experiments.

lyzing superoxide and hydrogen peroxide, respectively, prevented the doxorubicin-induced decrease of FLIP protein expression. Likewise, the antioxidant *N*-acetylcysteine (NAC) also restored the down-regulation of FLIP with doxorubicin treatment. Conversely, hydrogen peroxide, which is the most diffusible reactive oxygen species, itself decreases FLIP expression in a dose dependent manner. These results indicate that reactive oxygen species mediate the inhibitory action of doxorubicin on FLIP expression in cardiac myocytes. Following the reversal to the baseline level of FLIP by treatments with antioxidants, cardiac myocytes became resistant to Fas-mediated apoptosis again. Levels of FLIP have been demonstrated to play a pivotal role in the Fas-mediated apoptosis in various cell types [24–26,37]. Thus, reactive oxygen species produced by doxorubicin sensitize rat neonatal cardiac myocytes to Fas-mediated apoptosis at least partly by the way of down-regulating FLIP. In human Jurkat T cell lines, doxorubicin-induced apoptosis was reported to be independent of Fas signaling [38,39]. However in leukaemic cells [40], incubation with anti-Fas IgM antibody and doxorubicin augmented apoptotic responses as we demonstrated using neonatal rat cardiomyocytes in the present study. These data implicate that doxorubicin- and Fas-mediated apoptosis is cell specific events and may share some common components in signaling pathways leading to apoptosis. To our knowledge, precise mechanisms for the downregulation of FLIP by reactive oxygen species are still unknown. Transcriptional regulations and the protein stability or degradation of FLIP are suggested as possible mechanisms [41,42].

Besides doxorubicin-induced heart failure, reactive oxygen species have been shown to cause contractile failure and structural damage in various types of heart failure [43]. There may be a possibility that FLIP levels are down-regulated by reactive oxygen species in the myocardium of the failing heart. Recently, Imanishi et al. [44] observed that FLIP-positive cells rarely had fragmented DNA, while TUNEL-positive cells rarely contained FLIP in end-stage human hearts. Cardiac myocytes of the failing heart may be primed for apoptotic signal by FasL which has been reported to be elevated in patients with congestive heart failure [21] (Fig. 6). In the transgenic mouse overexpressing FasL in the heart, neither myocardial apoptosis nor necrosis occurred in the heart despite expression of Fas [45]. However, since the FLIP level should be unchanged in the transgenic mouse, the absence of apoptosis in the

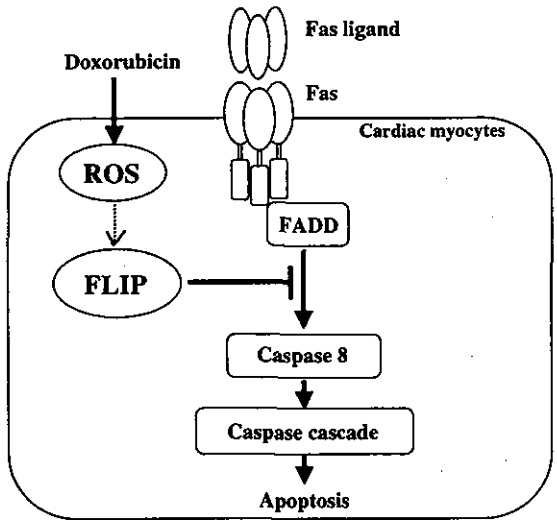

Fig. 6. One of proposed mechanism for doxorubicin-induced cardiomyopathy. Administration of doxorubicin produces reactive oxygen species (ROS) in cardiac myocytes and the ROS down-regulates the expression of FLIP that acts in a dominant-negative manner to inhibit caspase-8. In addition to increased level of Fas, the down-regulated FLIP renders cardiac myocytes Fas-sensitive, resulting in apoptosis. Fas ligand (FasL) may be expressed by leukocytes, cardiac myocytes and endothelial cells following administration of doxorubicin. FADD, Fas-associated death domain.

FasL-enforced myocardium might be due to relatively high FLIP levels.

In conclusion, FLIP contributes, at least in part, to doxorubicin-induced susceptibility to Fas-mediated apoptosis in cardiac myocytes. Importantly, the expression of FLIP is regulated by reactive oxygen species in cardiac myocytes.

Acknowledgements

This study was supported by grants from the Ministry of Education, Science and Culture, Japan (10307016 and 12670645).

References

[1] Singal PK, Iliskovic N. Doxorubicin-induced cardiomyopathy. New Engl J Med 1998;339:900–905.
[2] Singal PK, Deally MR, Weiberg LE. Subcellular effects of adriamycin in the heart: a concise review. J Mol Cell Cardiol 1987;19:817–828.
[3] Raju J, Coralie P, Hung-yi W et al. Molecular mechanisms of doxorubicin-induced cardiomyopathy; selective suppression of Reiske iron–sulfur protein, ADP/ATP translocate, and phosphofructokinase genes is associated with ATP depletion in rat cardiomyocytes. J Biol Chem 1997;272:5828–5832.
[4] Lee V, Randhawa AK, Singal PK. Adriamycin-induced myocardial dysfunction in vitro is mediated by free radicals. Am J Physiol 1991;261:H989–995.
[5] Kawano H, Okada R, Kawano Y et al. Apoptosis in acute and chronic myocarditis. Jpn Heart J 1994;35:745–750.
[6] Itoh G, Tamura J, Suzuki Y et al. DNA fragmentation of human infarcted myocardial cells demonstrated by the nick end labeling method and DNA agarose gel electrophoresis. Am J Pathol 1995;146:1325–1331.
[7] Mallat Z, Tedgui A, Fontaliran F et al. Evidence of apoptosis in arrhythmogenic right ventricular dysplasia. New Engl J Med 1996;335:1190–1196.
[8] Olivetti G, Abbi R, Quaini F et al. Apoptosis in the failing heart failure. New Engl J Med 1996;336:1131–1141.
[9] Nagata S. Apoptosis by death factor. Cell 1997;88:355–365.
[10] Tanaka M, Ito H, Adachi S et al. Hypoxia induces apoptosis with enhanced expression of Fas antigen messenger RNA in cultured neonatal rat cardiomyocytes. Circ Res 1994;75:426–433.
[11] Suda T, Takahashi T, Golstein P et al. Molecular cloning and expression of the Fas ligand, a novel member of the tumor necrosis factor family. Cell 1993;75(6):1169–1178.
[12] Arase H, Arase N, Saito T. Fas-mediated cytotoxicity by freshly isolated natural killer cells. J Exp Med 1995;181:1235–1238.
[13] Sata M, Walsh K. TNF alpha regulation of Fas expression on endothelium modulates leukocyte infiltration of the blood vessel wall. Nature Med 1998;4:415–420.
[14] Griffith TS, Brunner T, Fletcher SM et al. Fas ligand-induced apoptosis as a mechanism of immune privilege. Science 1995;270:1189–1192.
[15] Tanaka M, Suda T, Takahashi T, Nagata S. Expression of the functional soluble form of human fas ligand in activated lymphocytes. EMBO J 1995;14(6):1129–1135.
[16] Tanaka M, Suda T, Yatomi T, Nakamura N, Nagata S. Lethal effect of recombinant human Fas ligand in mice pretreated with *Propionibacterium* acnes. J Immunol 1997;158(5):2303–2309.
[17] Song E, Chen J, Ouyang N et al. Soluble Fas ligand released by colon adenocarcinoma cells induces host lymphocyte apoptosis: an active mode of immune evasion in colon cancer. Br J Cancer 2001;85(7):1047–1054.
[18] Tanaka M, Itai T, Adachi M, Nagata S. Downregulation of Fas ligand by shedding. Nature Med 1998;4(1):31–36.
[19] Nishigaki K, Minatoguchi S, Seishima M et al. Plasma Fas ligand, an inducer of apoptosis, and plasma soluble Fas, an inhibitor of apoptosis, in patients with chronic congestive heart failure. J Am Coll Cardiol 1997;29:1214–1220.
[20] Okuyama M, Yamaguchi S, Nozaki N et al. Serum levels of soluble form of Fas molecule in patients with congestive heart failure. Am J Cardiol 1997;79(12):1698–1701.
[21] Yamaguchi S, Yamaoka M, Okuyama M et al. Elevated circulating levels and cardiac secretion of soluble Fas ligand in patients with congestive heart failure. Am J Cardiol 1999;83:1500–1503.
[22] Nakamura T, Ueda Y, Juan Y et al. Fas-mediated apoptosis in adriamycin-induced cardiomyopathy in rats. Circulation 2000;102:572–578.
[23] Yamaoka M, Yamaguchi S, Suzuki T et al. Apoptosis in rat cardiac myocytes induced by Fas ligand: priming for Fas-mediated apoptosis with doxorubicin. J Mol Cell Cardiol 2000;32:881–889.
[24] Thome M, Schneider P, Hofmann K et al. Viral FLICE-inhibitory proteins (FLIPs) prevent apoptosis induced by death receptors. Nature 1997;386:517–521.
[25] Hu S, Vincenz V, Buller M, Dixit VM. A novel family of viral death effector domain-containing molecules that inhibit both CD-95 and tumor necrosis factor receptor-1-induced apoptosis. J Biol Chem 1997;272:9621–9624.
[26] Irmler M, Thome M, Hahne M et al. Inhibition of death receptor signals by cellular FLIP. Nature 1997;388:190–195.
[27] Takahashi T, Tanaka M, Inazawa J et al. Human Fas Ligand: gene structure, chromosomal location and species specificity. Int Immunol 1994;6:1567–1574.
[28] Suda T, Nagata S. Purification and characterization of the Fas-ligand that induces apoptosis. J Exp Med 1994;179:873–879.

[29] Sata M, Kenneth W. Endothelial cell apoptosis induced by oxidized LDL is associated with the down-regulation of the cellular caspase inhibitor FLIP. J Biol Chem 1998;273:33103–33106.
[30] Zulfiqar FC, Stepen BW, Masataka S et al. Fas/Apo-1 and associated proteins in the differentiating cerebral cortex: induction of caspase-dependent cell death and activation of NF-kB. J Neurosci 1999;19:1754–1770.
[31] Tanaka M, Suda T, Haze K et al. Fas ligand in human serum. Nature Med 1996;2:317–322.
[32] Niehaus WG, Samuelsson B. Formation of malonaldehyde from phospholipid arachidonate during microsomal lipid peroxidation. Eur J Biochem 1968;6:126–132.
[33] Tobin TP, Abbott BC. A stereological analysis of the effect of adriamycin on the ultrastructure of rat myocardial cells in culture. J Mol Cell Cardiol 1980;12:1207–1225.
[34] Sawyer DB, Fukazawa R, Arstall MA et al. Daunorubicin-induced apoptosis in rat cardiac myocytes is inhibited by dexrazoxane. Circ Res 1999;84:257–265.
[35] Timao L, Singal PK. Adriamycin-induced early changes in myocardial antioxidant enzymes and their modulation by probucol. Circulation 2000;102:2105–2110.
[36] Negoro S, Oh H, Tone E et al. Glycoprotein 130 regulates cardiac myocyte survival in doxorubicin-induced apoptosis through phosphatidylinositol 3-kinase/Akt phosphorylation and Bcl-xL/caspase-3 interaction. Circulation 2001;103:555–561.
[37] Scaffidi C, Schmitz I, Krammer PH et al. The role of c-FLIP in modulation of CD95-induced apoptosis. J Biol Chem 1999;274:1541–1548.
[38] Kataoka T, Schroter M, Hahne M et al. FLIP prevent apoptosis induced by death receptors but not by perforin/granzyme B, chemotherapeutic drugs, and gamma irradiation. J Immunol 1998;161:3936–3942.
[39] Wesselborg S, Engels IH, Rossmann E, Los M, Schulze-Osthoff K. Anticancer drugs induce caspase-8/FLICE activation and apoptosis in the absence of CD95 receptor/ligand interaction. Blood 1999;93:3053–3063.
[40] Mcgahon AJ, Pereira AP, Daly L, Cotter TG. Chemotherapeutic drug-induced apoptosis in human leukaemic cells in independent of the Fas (APO-1/CD95) receptor/ligand system. Br J Haematol 1998;101:539–547.
[41] Yeh JH, Hsu SC, Han SH et al. Mitogen-activated protein kinase kinase antagonized Fas-associated death domain protein-mediated apoptosis by induced FLICE-inhibitory protein expression. J Exp Med 1998;188:1795–1802.
[42] Panka DJ, Mano T, Suhara T et al. Phosphatidylinositol-3 kinase/akt activity regulates c-FLIP expression in tumor cells. J Biol Chem 2001;276(10):6893–6896.
[43] Singal PK, Khaper N, Palace V et al. The role of oxidative stress in the genesis of heart disease. Cardiovasc Res 1998;40:426–432.
[44] Imanishi T, Murry CE, Reinecke H et al. Cellular FLIP is expressed in cardiomyocytes and down-regulated in TUNEL-positive grafted cardiac tissues. Cardiovasc Res 2000;48:101–110.
[45] Nelson DP, Setser E, Hall DG et al. Proinflammatory consequences of transgenic Fas ligand expression in the heart. J Clin Invest 2000;105:1199–1208.

Inhibition of Experimental Intimal Thickening in Mice Lacking a Novel G-Protein–Coupled Receptor

Shuichi Tsukada, MSc; Masaru Iwai, MD, PhD; Jun Nishiu, MSc; Makoto Itoh, MD, PhD; Hitonobu Tomoike, MD, PhD; Masatsugu Horiuchi, MD, PhD; Yusuke Nakamura, MD, PhD; Toshihiro Tanaka, MD, PhD

Background—Vascular restenosis attributable to intimal thickening remains a major problem after percutaneous transluminal coronary angioplasty (PTCA).

Methods and Results—Through differential-display analysis, we have identified a novel gene whose expression was increased after catheter injury of rabbit aorta. The gene that is expressed predominantly in vascular smooth muscle cells encodes a novel protein with 7 transmembrane domains, and we termed it *ITR* (intimal thickness–related receptor). The *ITR* sequence contains a motif common to the Rhodopsin-like GPCR (G-protein-coupled receptor) superfamily. In vivo analyses of this gene revealed that expression of ITR protein increased with intimal thickening induced by cuff placement around murine femoral artery. Furthermore, *ITR*-knockout mice were found to be resistant to this experimental intimal thickening.

Conclusions—*ITR* thus seems to be a novel receptor that may play a role in vascular remodeling and that may represent a good target for development of drugs in the prevention of vascular restenosis.

Key Words: angioplasty ■ genes ■ restenosis

Percutaneous transluminal coronary angioplasty (PTCA) is a widely used therapeutic procedure for coronary artery diseases, including angina pectoris and myocardial infarction. However, restenosis, which occurs in 30% to 50% of patients after PTCA as a consequence of cellular hyperplasia within the neointima, is an issue of clinical urgency. Cell-cell interactions, cell-matrix interactions, redox state, ligand-receptor interactions, tyrosine kinases, and transcription factors are all involved in endothelial dysfunction and formation of neointima.[1] However, only a few genes have been reported in relation to this highly complex phenomenon.

Genes encoding G-protein–coupled receptors (GPCRs) represent the largest superfamily yet identified; more than 800 of them have been discovered to date from a wide range of species. A characteristic motif of gene products in this superfamily is the presence of 7 distinct hydrophobic regions, each 20 to 30 amino acids in length, that are generally regarded as the transmembrane domains of these integral membrane proteins. There is little conservation of amino acid sequence across the entire superfamily of receptors, but key sequence motifs can be found within phylogenetically related subfamilies.[2–6] GPCRs are excellent drug targets, and in fact several hundred drugs launched within the past 3 decades are directed to known GPCRs.[7–10] Therefore, any GPCR whose expression level is changed when vascular smooth muscle cells (VSMCs) are multiplying would be a promising target molecule for prevention of restenosis.

We had performed differential mRNA display analyses[11] of a rabbit model of vascular injury to identify genes that were upregulated or downregulated after denudation by a balloon catheter.[12] In the present study, we report isolation and characterization of a novel gene, designated *ITR*, that was upregulated in the acute phase after balloon injury of the rabbit aorta.

Methods

Cloning of Full-Length cDNA

To isolate a full-length rabbit ITR gene, 5′-RACE was performed using the Marathon cDNA Amplification Kit (Clontech Laboratories). Full-length cDNAs of human, mouse, and rat orthologs were cloned by screening heart cDNA libraries of each species (Clontech).

RNA Expression of the Human ITR Gene

For Northern blot analysis, human multiple-tissue Northern blot (CLONTECH) was hybridized to [^{32}P]dCTP-labeled full-length human ITR cDNA. All blots were washed at 0.1× SSC, 65°C, and exposed to autoradiography film overnight. Total RNAs were isolated from human umbilical vein endothelial cells, human coronary artery endothelial cells, and human coronary artery smooth muscle cells. Reverse transcriptase–polymerase chain reaction (RT-PCR) was performed using a set of primers, hITR-RTF

Received July 2, 2002; revision received September 6, 2002; accepted September 13, 2002.

From the Laboratory of Molecular Medicine, Human Genome Center, Institute of Medical Science, University of Tokyo (S.T., J.N., M. Itoh, Y.N., T.T.), Department of First Medical Biochemistry, Ehime University School of Medicine (M. Iwai, M.H.), and First Department of Internal Medicine, Yamagata University School of Medicine (M. Itoh, H.T.), Japan.

Correspondence to Yusuke Nakamura, Laboratory of Molecular Medicine, Human Genome Center, Institute of Medical Science, University of Tokyo, 4-6-1, Shirokanedai, Minato-ku, Tokyo 108-8639, Japan. E-mail yusuke@ims.u-tokyo.ac.jp

Circulation is available at http://www.circulationaha.org

DOI: 10.1161/01.CIR.0000043804.29963.B4

(5′-TGGCATTGCAGTATTCATTG-3′) and hITR-RTR (5′-CAGACTGGCAAAGGATAACAC-3′).

Chromosomal Localization of the Human ITR Gene

The human genomic cosmid clone was isolated from a human genomic DNA library (STRATAGENE, Gebouw) using the human full-length cDNA as a probe and used for the FISH experiment on a R-banded metaphase spreads, as described previously.[13–15] More than 100 metaphase cells were examined after in situ hybridization.

Computer Analysis and Database Search

Using the FASTA program,[16] we compared nucleotide and deduced amino acid sequences to the respective databases (nonredundant combination of GenBank, EMBL, and DDBJ databases for nucleotides and the nonredundant combination of Swiss-prot, PIR, and PRF databases plus translations of DNA sequences in GenBank for amino acids). A motif search was done at PRINTS.[17]

Generation of Mice Lacking ITR

An *ITR*-targeting plasmid was constructed according to a method based on inverse-PCR described previously.[18] To isolate BAC clones containing the mouse ITR gene, "down to the well mouse ES BAC DNA pool" (Genome Systems Inc, St Louis, Mo) was screened by the primer pair ITR-BACF (5′-CCGATGATTGGTTACTGTCCCCG-3′) and ITR-BACR (5′-CCGATGATTGGTTACTGTCCCCG-3′), corresponding to DNA sequences in exon 1. A 2-μg aliquot of isolated BAC DNA was digested with *Hind*III, circularized by self-ligation at 4°C for 16 hours, and used as template for inverse-PCR. Amplification was performed by the primer pair ITR-KI5′ (5′-ACGCGTTTAATTAAGTCGGCAGCAGAGGGCGGGGCGGGACTTAG-3′) and ITR-KI3′ (5′-ACGCGTGCGGCCGCGCATTCGAGCCCTGTGGTTATGAGTGGATG-3′). After digesting both ends of PCR product with *Not*I and *Pac*I, the DNA fragment was cloned into p1108 vector and linearized by *Hind*III digestion before transfection. Targeting of the ITR gene and generation of knockout mice using E14.1 embryonic stem (ES) cells (129/SVJ) were performed by essentially standard techniques.[19] Animals considered to be chimeric on the basis of their coat colors were mated with 129/SVJ or C57BL/6J mice. DNA samples were isolated from tails of ES cell-derived animals for genotyping. ES cells and F1 mice were analyzed for the presence of a disrupted ITR gene by Southern blot analysis. F2 mice genotyping was done by PCR using tail genomic DNA as a template and the following three primers: primer 1 specific for wild-type allele (5′-CCGTTTCCATTTCCCCGACAC-3′), primer 2 specific for recombinant allele (5′-CTCCAAAAAAGCCTCCTCACT-3′), and primer 3 for both alleles (5′-CGGTCTTACAAACAACAGGGA-3′).

Preparation of Anti-ITR Monoclonal Antibody

COS7 cells were transfected with pFLAG-CMV-1 vector to design to express *N*-terminal portion of rat ITR (rN-ITR) corresponding to the extracellular domain, and the induced protein was purified with anti-FLAG affinity column. Anti-ITR monoclonal antibody (Mab) was prepared by immunizing female BALB/c mice (Shizuoka Laboratory Animal Center, Shizuoka, Japan) every seventh day with a footpad injection of purified rN-ITR. The booster injection was made into the footpad 2 days before fusion. Popliteal lymph node cells were fused with mouse myeloma cells, PAI, using PEG4000 (Life Technologies, Inc), and the resulting hybridomas were screened according to their ability to stain ITR transfectants.

Cuff-Induced Intimal Thickening of the Murine Femoral Artery

Adult male mice (n=10) lacking *ITR* and 10- to 12-week-old WT male mice (n=9) from the same genetic background were housed under climate-controlled conditions with a 12-hour light/dark cycle, with room temperature kept at 25°C. They were given a standard diet (MF, Oriental Yeast Co Ltd) and water ad libitum. The experimental protocol was approved by the Animal Studies Committee of Ehime University. Surgery to place polyethylene cuffs (2-mm long PE-90; Becton-Dickinson) and to obtain artery samples was performed according to methods described previously.[20–23] Excised arterial tissues were fixed in 10% formalin overnight, dehydrated, and embedded in paraffin.

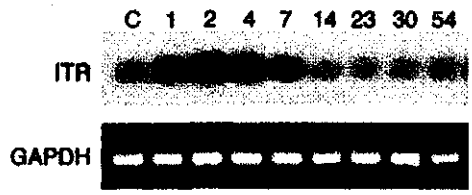

Figure 1. Expression of ITR mRNA in rabbits after balloon injury, examined by RT-PCR. Numerals indicate days after injury, and C denotes intact aorta. Glyceraldehyde-3-phosphate dehydrogenase (GAPDH) was used as an internal control.

The middle segment of artery from each mouse was cut into 3 subserial cross sections of 5-μm thickness at intervals of 0.3 mm. The sections were stained by Elastica van Gieson staining to investigate overall morphology and photography. The areas covered by neointima and media were measured using image-analyzing software (NIH image). Neointima was defined as the area between the vessel lumen and the internal elastic lamina. Media was defined as the area between the internal and external elastic lamina. The average of 3 sections was taken as the value for each animal.

The artery samples were taken 7 days after cuff placement, and bromodeoxyuridine (BrdU, Sigma) was injected 100 mg/kg SC and 30 mg/kg IP at 18 hours before euthanasia and then 30 mg/kg IP at 12 hours before euthanasia.[20,21] The sections were prepared in the same manner as morphometric analysis. Immunohistochemistry using anti-BrdU antibody was performed according to the manufacturer's protocol (BrdU Staining Kit; Zymed Laboratories). After the sections were counterstained with hematoxylin, we calculated the BrdU index (the ratio of BrdU-positive nuclei versus total nuclei). The average index of 3 sections was taken as the value for each animal. Statistical analyses were performed using two-way ANOVA. When a significant effect was found, post-hoc analysis was done to detect the difference between the groups. $P<0.05$ was considered statistically significant.

Immunohistochemical Staining of ITR

ITR in the cuffed artery was stained with mouse-to-mouse staining kit (M.O.M. Immunodetection kit, Vector Laboratories) using formalin-fixed, paraffin-embedded sections. Endogenous peroxidase was blocked by 0.3% hydrogen peroxide in methanol. Primary antibody was applied to the sections and incubated for 16 to 24 hours at 4°C. Positive staining was visualized using diaminobenzidine, and counterstained nuclei with hematoxylin.

Results

Cloning and Characterization of the ITR Gene

Using a differential mRNA display method, we isolated a novel cDNA fragment that was upregulated early after injury of the rabbit aorta. Because the clone covered only part of the 3′-untranslated region, 5′ and 3′ rapid amplification of cDNA ends (RACE) experiments were performed to isolate the full-length cDNA, which we named *ITR*. RT-PCR showed that expression of this rabbit mRNA was significantly elevated 2 or 4 days after injury of the aorta and declined afterward (Figure 1). This result was confirmed by a similar procedure using carotid arteries from rats (data not shown).

Human, mouse, and rat counterparts of the rabbit *ITR* were isolated from cDNA libraries of the respective species. Alignment of human, mouse, rabbit, and rat amino acid sequences deduced from their nucleotide sequences showed at least 80% identity among all 4 species. Each predicted amino acid sequence revealed a signal sequence at the amino-terminus and 7

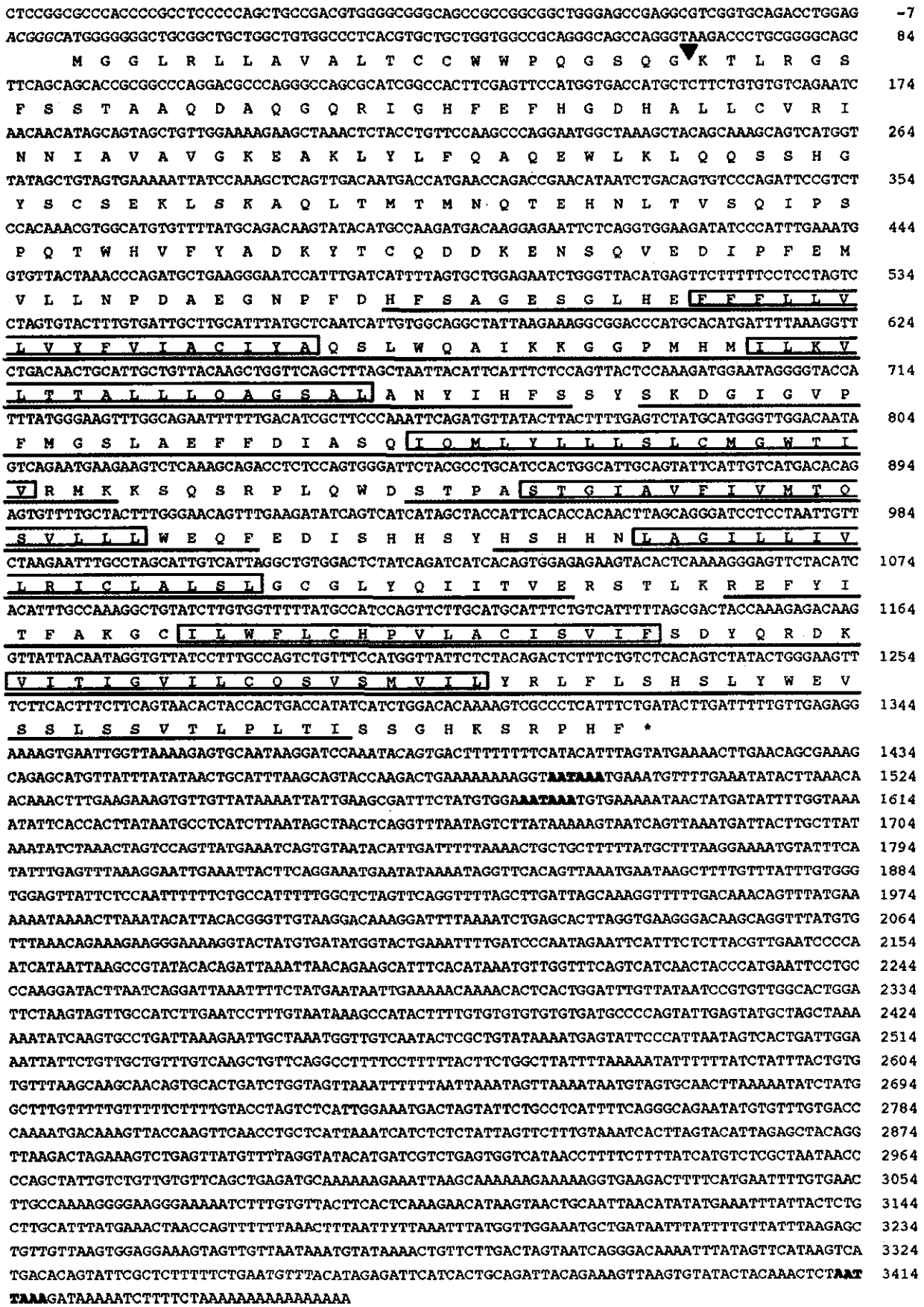

Figure 2. Nucleotide and predicted amino acid sequences of human ITR gene. Predicted signal sequence cleavage site is shown by a triangle, and 7 transmembrane regions are boxed. Three polyadenylation sites are indicated by boldface type. Rhodopsin-like GPCR superfamily signatures (GPCRRHODOPSN4 motif) are underlined. Kozak sequence adjacent to initiation codon is shown by italics.

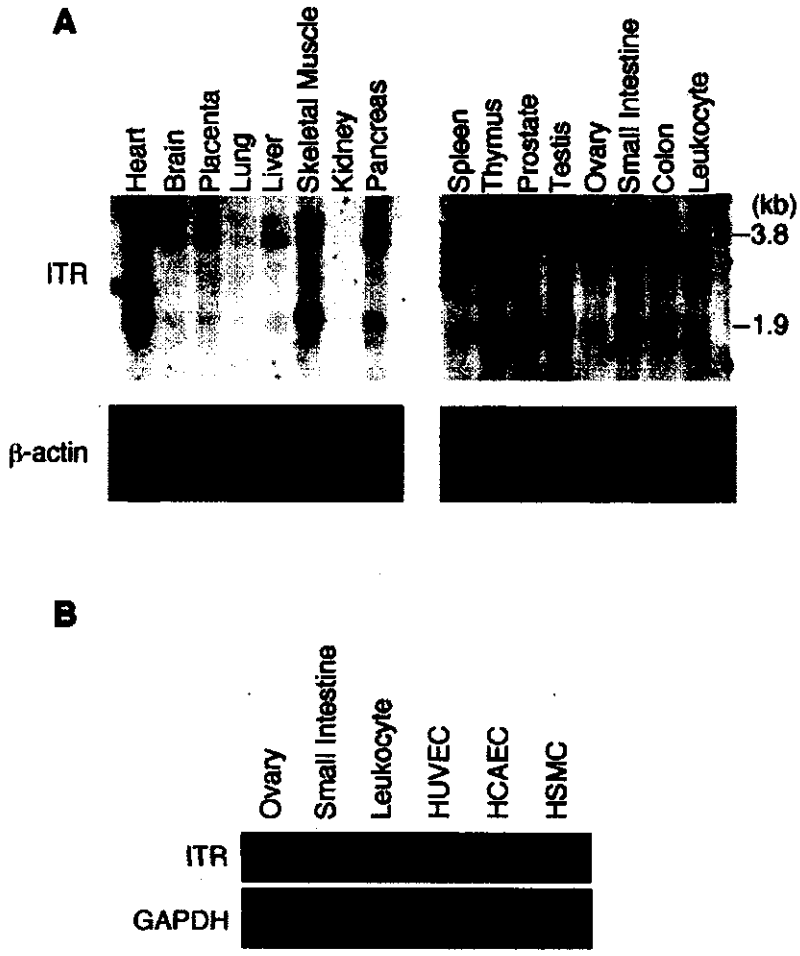

Figure 3. A, Northern-blot analysis of human ITR mRNA. Blots from various adult human tissues containing 2 μg of poly(A) RNA in each lane were probed with human ITR cDNA. The bottom panel shows the same blot hybridized with β-actin. B, Expression of ITR mRNA in each of the cell types that constitute blood vessel. HUVEC, HCAEC, and HSMC represent human umbilical vein endothelial cells, human coronary artery endothelial cells, and human coronary artery smooth muscle cells, respectively. Other types of tissues serve as controls to compare the results of Northern blot analysis. Glyceraldehyde-3-phosphate dehydrogenase (GAPDH) was used as a control.

transmembrane regions in the center. A search for motifs in the ITR protein revealed GPCRRHODOPSN4, a signature of the Rhodopsin-like GPCR superfamily (Figure 2).

The ITR gene was ubiquitously expressed in normal human tissues on Northern blots, where 2 transcripts (approximate molecular sizes, 1.9 and 3.8 kb) were detected in the tissues analyzed (Figure 3A), owing probably to the different sites of polyadenylation seen in Figure 2. We also examined expression pattern of this gene among cells constituting blood vessel and found that this gene was predominantly expressed in smooth muscle cells (Figure 3B).

The chromosomal localization of the human ITR gene was determined by fluorescence in situ hybridization using a full-length human ITR cDNA as the probe. Metaphase cells showed specific hybridization signals with twin spots at chromosomal band 13q31 (data not shown).

Role of ITR in Vascular Remodeling

To investigate the in vivo role of ITR, we generated mice lacking this gene (see Figure 4 for targeting scheme). Under normal conditions, ITR-null mice were indistinguishable from wild-type mice in appearance, growth rate, reproduction, and histology of major organs, including liver, heart, lung, brain, aorta, kidney, thymus, testis, muscle, pancreas, or spleen. To elucidate the in vivo role of *ITR* in intimal thickening, we performed cuff placement experiment around mouse femoral artery. As shown in Figure 5A, intimal thickening was observed 14 days after surgery in wild-type mouse. Immunohistochemical staining revealed that expression of ITR protein was induced in media and intima of the injured artery at 7 days after cuff placement, when intimal thickening was not yet overt (Figure 6). On the other hand, ITR-null mice hardly showed any of the neointima that were formed in wild-type mice during the experimental period (Figure 5A). The neointimal area was ≈200% greater in wild-type mouse than in ITR-null mouse 14 days after cuff placement ($P<0.01$, Figure 5B and 5D). There was no significant difference in the medial area between wild-type and ITR-null mice (Figure 5C). As a marker of DNA synthesis in vascular smooth muscle cell (VSMC), BrdU incorporation into VSMC after cuff placement was significantly suppressed in ITR-null mice ($P<0.001$, Figure 5E).

Discussion

We have described here the cloning and characterization of a putative G-protein–coupled receptor, called *ITR*, that was isolated as a novel gene differentially expressed at an early phase of vascular injury in rabbits.

The deduced amino acid sequence of *ITR* contains a secondary structure of 7 transmembrane α-helical domains characteristic of the Rhodopsin-like GPCR superfamily. GPCRs represent an increasingly large and functionally diverse superfamily of receptors whose intracellular actions are mediated by signaling pathways involving G proteins and downstream secondary

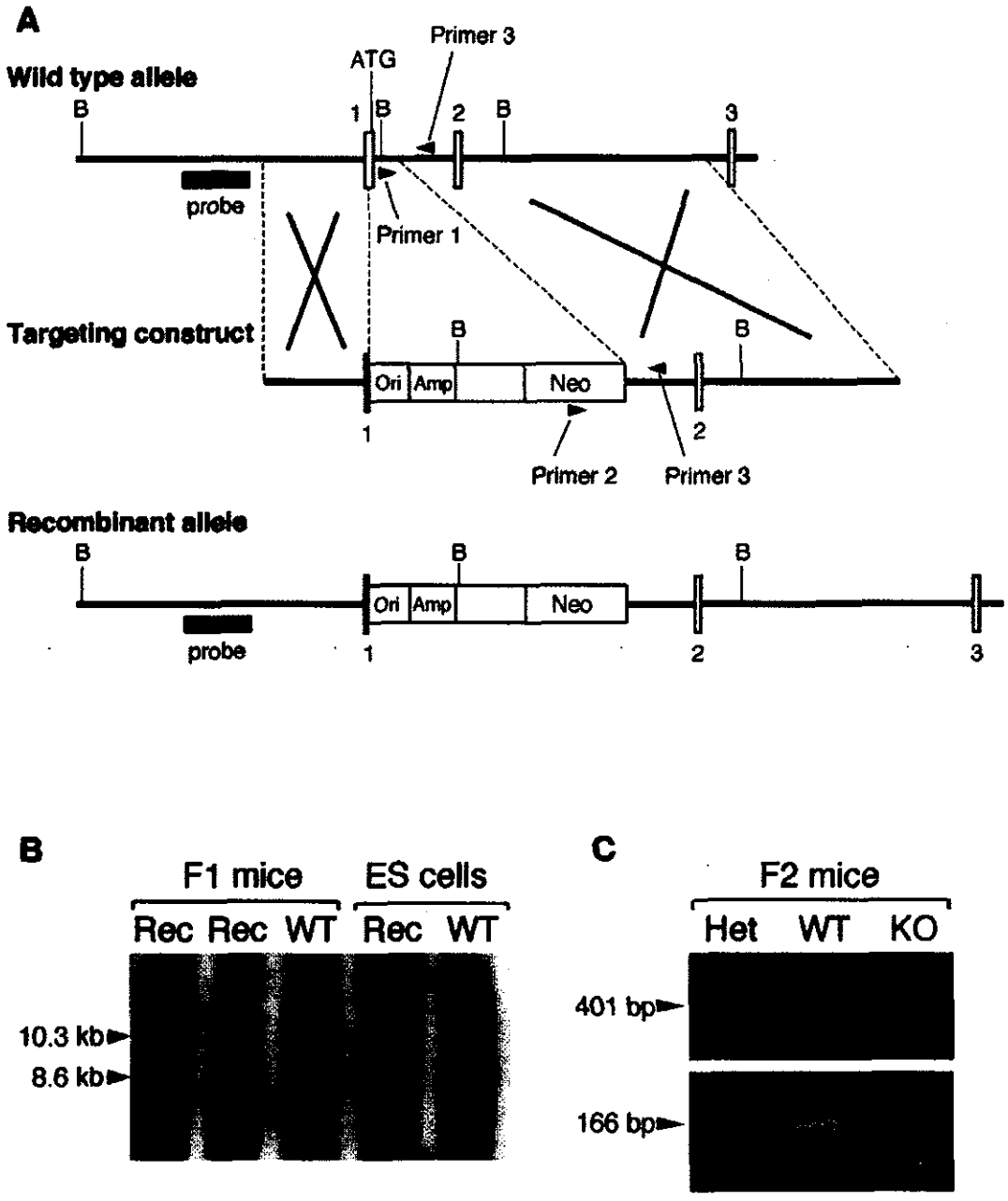

Figure 4. Generation of ITR-deficient mice by gene targeting. A, ITR gene was disrupted by replacing part of exon 1 and intron 1 with the neomycin-resistance cassette. B, Southern blot analysis of genomic DNA from ES cells and F1 mice using probes outside the homologous recombination region, as indicated in panel A. C, Genotyping of F2 mice by means of PCR. For the presence of recombinant allele, primer 2 and primer 3 were used (top), and for wild-type allele, primer 1 and primer 2 were used (bottom).

messengers.[2-4] Receptors of this class respond to a variety of extracellular signals, including peptide hormones, lipid-derived messengers, and neurotransmitters. Because 7 transmembrane domains are present in all GPCRs, most of these receptors bear sequence similarity to one another, primarily in the transmembrane regions.[5,6,24,25] However, *ITR* has little sequence homology to any known proteins, although its putative transmembrane domains do contain signatures of the Rhodopsin-like GPCR superfamily. Therefore, ITR protein may be an orphan GPCR rather than a member of any known GPCR subfamily. The lack of sequence homology to other known GPCRs makes it difficult to predict the specific ligand for this receptor or the identities of its coupled G protein and second messengers.

We performed two distinct experiments to study pathogenesis of intimal thickening; one was the catheter injury of rabbit aorta and the other was the cuff placement around mouse femoral artery. In both models, expression of ITR was induced before intimal thickening became overt. Combining our results that ITR was predominantly expressed in vascular smooth muscle cell and that *ITR*-deficient mice were resistant to this experimental intimal thickening, it may be reasonable to suggest that ITR is essential in the early stage of intimal thickening, especially for vascular smooth muscle cells to receive one of the critical signals to migrate or proliferate.

Because ITR is a putative GPCR, it may be a good target for drug development to encounter intimal thicken-

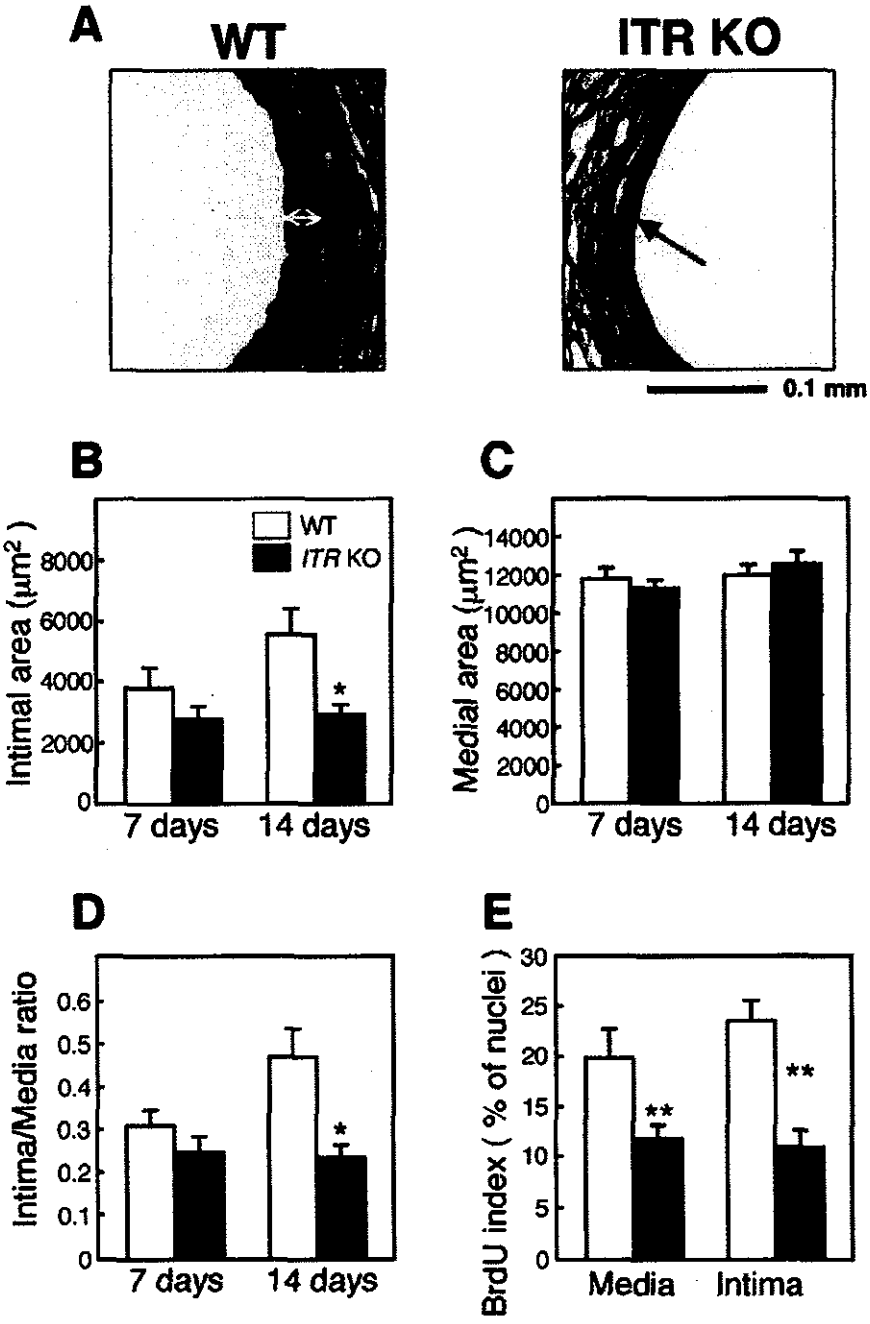

Figure 5. Morphometric analysis of injured artery after placement of polyethylene-cuff in wild-type (WT) and ITR-null (ITR KO) mice. A, Elastica van Gieson staining of cuffed femoral artery 14 days after cuff placement. Magnification ×50. Artery samples were obtained 7 days and 14 days after cuff placement. B, Intimal area; C, Medial area; D, Intima/media ratio. *$P<0.01$ versus WT. Values are mean±SEM. E, Bromodeoxyuridine (BrdU) incorporation in media and neointima of cuffed femoral artery. BrdU index (BrdU-positive nuclei/total nuclei) was analyzed 7 days after surgery. **$P<0.001$ vs WT. Values are mean±SEM.

ing, although the relevance of our findings in human remains to be clarified. Isolation of its ligand may provide an important clue for a better understanding of its pathogenesis.

Acknowledgments

This work was supported in part by Research for the Future Program Grant No. 00 L 01402 from the Japan Society for the Promotion of Science.

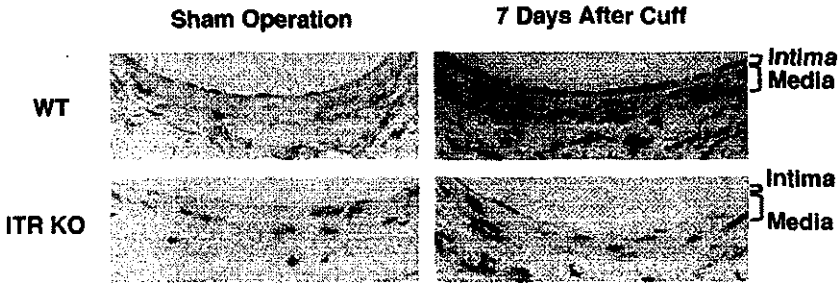

Figure 6. Immunohistochemical staining of ITR in injured artery 7 days after cuff placement. Artery samples were obtained from wild-type (WT) and ITR-null (ITR KO) mice, and paraffin-sections of arteries were stained with monoclonal antibody for ITR.

References

1. Gibbons GH, Dzau VJ. Molecular therapies for vascular diseases. *Science*. 1996;272:689–693.
2. Dohlman HG, Thorner J, Caron MG, et al. Model systems for the study of seven-transmembrane-segment receptors. *Annu Rev Biochem*. 1991; 60:653–688.
3. Wess J. G-protein-coupled receptors: molecular mechanisms involved in receptor activation and selectivity of G-protein recognition. *FASEB J*. 1997;11:346–354.
4. Baldwin JM. Structure and function of receptors coupled to G proteins. *Curr Opin Cell Biol*. 1994;6:180–190.
5. Rohrer DK, Kobilka BK. G protein-coupled receptors: functional and mechanistic insights through altered gene expression. *Physiol Rev*. 1998;78 35–53.
6. Gether U. Uncovering molecular mechanisms involved in activation of G protein-coupled receptors. *Endocrine Rev*. 2000;21:90–113.
7. Stadel JM, Wilson S, Bergsma DJ. Orphan G protein-coupled receptors: a neglected opportunity for pioneer drug discovery. *Trends Pharmacol Sci*. 1997;18:430–437.
8. Wilson S, Bergsma DJ, Chambers JK. et al. Orphan G-protein-coupled receptors: the next generation of drug targets? *Br J Pharmacol*. 1998; 125:1387–1392.
9. Howard AD, McAllister G, Feighner SD, et al. Orphan G-protein-coupled receptors and natural ligand discovery. *Trends Pharmacol Sci*. 2001;22: 132–140.
10. Zhong H, Neubig RR. Regulators of G protein signaling proteins: novel multifunctional drug targets. *J Pharmacol Exp Ther*. 2001;297:837–845.
11. Ozaki K, Kuroki T, Hayashi S, et al. Isolation of three testis-specific genes (TSA303, TSA806, TSA903) by a differential mRNA display method. *Genomics*. 1996;36:316–319.
12. Itoh M, Tsukada S, Orita T, et al. Identification by differential display of eight known genes induced during in vivo intimal hyperplasia. *J Hum Genet*. 1998;43:9–13.
13. Inazawa J, Saito H, Ariyama T, et al. High-resolution cytogenetic mapping of 342 new cosmid markers including 43 RFLP markers on human chromosome 17 by fluorescence in situ hybridization. *Genomics*. 1993;17:153–162.
14. Pinkel D, Straum T, Gray JW. Cytogenetic analysis using quantitative, high-resolution, fluorescent in situ hybridization. *Proc Natl Acad Sci USA*. 1986;83:2934–2938.
15. Takahashi E, Hori T, O'Connell P, et al. R-banding and nonisotopic in situ hybridization: precise localization of the human type II collagen gene (COL2A1). *Hum Genet*. 1990;86:14–16.
16. Pearson WR, Lipman DJ. Improved tools for biological sequence comparison. *Proc Natl Acad Sci USA*. 1988;85:2444–2448.
17. Attwood TK, Flower DR, Lewis AP, et al. PRINTS prepares for the new millennium. *Nucleic Acids Res*. 1999;27:220–225.
18. Akiyama K, Watanabe H, Tsukada S, et al. A novel method for constructing gene-targeting vectors. *Nucleic Acids Res*. 2000;28:E77. Available at http://nar.oupjournals.org/cgi/content/full/28/16/e77. Accessed Novemer 26, 2002.
19. Joyner AL, ed. *Gene Targeting: A Practical Approach*. Oxford: Oxford University Press; 1993:33–61.
20. Akishita M, Horiuchi M, Yamada H, et al. Inflammation influences vascular remodeling through AT2 receptor expression and signaling. *Physiol Genomics*. 2000;2:13–20.
21. Wu L, Iwai M, Nakagami H, et al. Roles of AT_2 receptor stimulation associated with selective AT_1 receptor blockade with valsartan in the improvement of inflammation-induced vascular injury. *Circulation*. 2001;27:104:2716–2721.
22. Mori M, Zhang L, Yasuda T, et al. Interaction of genetic deficiency of endothelial nitric oxide, gender, and pregnancy in vascular response to injury in mice. *J Clin Invest*. 1998;101:1225–1232.
23. Hirosumi J, Nomoto A, Ohkubo Y, et al. Inflammatory responses in cuff-induced atherosclerosis in rabbits. *Atherosclerosis*. 1987;64: 243–254.
24. Probst WC, Snyder LA, Schuster DI, et al. Sequence alignment of the G-protein coupled receptor superfamily. *DNA Cell Biol*. 1992;11:1–20.
25. Horn F, Weare J, Beukers MW, et al. GPCRDB: an information system for G protein-coupled receptors. *Nucleic Acids Res*. 1998;26:275–279.

Role of Nitric Oxide in the Progression of Cardiovascular Remodeling Induced by Carotid Arterio-Venous Shunt in Rabbits

Takuya MIYAMOTO,[1] MD, Yasuchika TAKEISHI,[1] MD, Tetsurou SHISHIDO,[1] MD, Hiroki TAKAHASHI,[1] MD, Makoto ITOH,[1] MD, Isao KUBOTA,[1] MD, *and* Hitonobu TOMOIKE,[2] MD

SUMMARY

Despite a variety of biological roles for nitric oxide (NO) in the cardiovascular system, little is known about whether NO is involved in cardiac hypertrophy. We hypothesized that NO production following a sustained increase in shear stress by volume-overload modifies the level of cardiac hypertrophy independent of hemodynamic changes. Volume-overload was induced by shunt formation between the left common carotid artery and the external jugular vein in 21 rabbits. These shunt rabbits were randomly assigned to 3 groups: shunt with no treatment (n=8), shunt treated with a low dose of N^G-nitro-L-arginine methyl ester (L-NAME, 0.5 g/L in drinking water, n=8), and shunt with a high dose of L-NAME (1.5 g/L, n=5). Eight sham operated rabbits were used as controls. Treatments were started immediately after operation and were continued for 6 weeks. Chronic volume-overload by shunt formation caused left ventricular dilatation and arterial enlargement proximal to the fistula. The relative wall thickness of the left ventricle was decreased, indicating eccentric cardiac hypertrophy. L-NAME elevated mean arterial blood pressure (P<0.01) and reduced the increment of cardiac output (P<0.05). L-NAME attenuated ventricular weight (P<0.01), ventricular cavity dilatation (P<0.01), and arterial enlargement (P<0.05). The re-capitulation of atrial natriuretic factor mRNA in the hypertrophied left ventricular myocardium by volume-overload was attenuated with L-NAME. In this model with chronic volume-overload, NO plays a pivotal role in the progression of cardiovascular remodeling by regulating the loading conditions of the heart.
(Jpn Heart J 2003; 44: 127-137)

Key words: Hypertrophy, Nitric oxide, Remodeling, Volume overload

THE heart and vessels remodel their structure to adapt to changes in mechanical loading conditions.[1,2] In vessels, mechanical forces elicited by blood flow (shear stress) and pressure (cyclic strain) cause the release of endothelium-derived nitric oxide (NO), which modifies the structure of the vessel.[1,3-5] Chronic increases in shear stress lead to vascular enlargement, and this process results in a reduction of shear stress toward normal. In contrast, chronic increases in cyclic strain accompany thickening of the vascular wall.[1,2] On the other hand, in the heart, chronic volume-overload leads to eccentric cardiac hypertrophy, whereas chronic pressure-overload causes concentric cardiac hypertrophy. However, the precise mechanisms for these morphological differences in response to mechanical overloads are not completely understood.

Recent studies have shown that chronic inhibition of NO synthesis by oral administration of L-arginine analogues such as N^G-nitro-L-arginine methyl ester (L-NAME) causes systemic arterial hypertension, coronary vascular remodeling and cardiac hypertrophy in rats.[6-8] However, it is unclear whether these structural changes observed in NO deficiency are a direct effect of NO deficiency because NO deficiency produced marked hypertension.[6-8] Although concomitant administration of an anti-hypertensive agent prevents L-NAME induced hypertension, there is still controversial about whether the resulting myocardial structural changes are unaltered or attenuated by these agents.[8-10] Recent studies suggest that the NO-cyclic GMP pathway inhibits cell growth *in vitro* in cell culture systems.[11-13]

The purpose of the present study was to investigate the role of NO in the pathogenesis of cardiovascular remodeling in a chronic volume-overload rabbit model.[14,15] We evaluated the effects of the NO synthase inhibitor L-NAME on cardiovascular remodeling in this animal model.

METHODS

Animals and study protocols: Japanese White male rabbits (Kumagai Shouten, Saitama, Japan) weighing between 2.2 and 2.5 kg were used in the present study. The animals were handled according to the animal welfare regulations of Yamagata University, and the study protocol was approved by the Animal Subjects Committee of Yamagata University. The study conformed with the *Guide for the Care and Use of Laboratory Animals* published by the US National Institute of Health.

Shunt formation between the left carotid artery and external jugular vein was performed in 21 rabbits as previously described.[14,15] Eight rabbits that underwent a sham operation served as controls. After the operation, the rabbits were kept in individual cages in an environmentally controlled facility at 25°C and 50-60% humidity with the lights on from 6:00 AM to 6:00 PM and were provided with a conventional stock diet (120 g/day, Labo-R-Grower, Nihon Nosan Kogyo

From [1] the First Department of Internal Medicine, Yamagata University School of Medicine, Yamagata, and [2] National Cardiovascular Center, Suita, Japan.

This study was supported in part by grants-in-aid for Scientific Research (No. 12557061 to H. T. and No. 12770337 to Y. T.) from the Ministry of Education, Science, Sports and Culture, Japan and grants from the Kanae Foundation, The Naito Foundation, and a Japan Heart Foundation Research Grant (Y. T.).

Address for correspondence: Takuya Miyamoto, MD, The First Department of Internal Medicine, Yamagata University School of Medicine, 2-2-2 Iida-Nishi, Yamagata, 990-9585, Japan.

Received for publication January 11, 2002.
Revised and accepted July 8, 2002.

Ltd., Tokyo). To evaluate the role of NO in cardiovascular remodeling, the rabbits were randomly assigned to 4 groups; 8 sham rabbits that received no treatment served as control, 8 shunt rabbits with no treatment, 8 shunt rabbits given L-NAME 0.5 g/L (low dose), and 5 shunt rabbits given L-NAME 1.5 g/L (high dose) in their drinking water.[16] Treatment was started on the day of the operation and continued for 6 weeks.

Echocardiography: Echocardiography was performed at 6 weeks after surgery. The rabbits were lightly anesthetized with an intravenous injection of sodium pentobarbital (10 mg/kg), placed in the left lateral *decubitus* position, and two-dimensional and M-mode echocardiograms at the papillary muscle level were recorded with a 7.5 MHz transducer using commercially available equipment (SSA260A; Toshiba Co., Ltd., Tochigi, Japan). M mode tracings were recorded at 100 mm/s, on which left ventricular chamber size and the thickness of the interventricular septum and the posterior wall were measured. End-diastolic and end-systolic points were determined at the maximal and minimal chamber sizes, respectively. Three cardiac cycles of successful data recordings were averaged, and the following parameters were calculated;

Fractional Shortening (%, FS)=(LVDd-LVDs)/LVDd×100

(LVDd, left *ventricular dimension* at end-diastole; LVDs, left ventricular dimension at end-systole)

Relative Wall Thickness (RWT)=2×Posterior Wall Thickness/LVDd

Hemodynamic measurements: After treatment for 6 weeks, all of the rabbits were anesthetized with an intravenous injection of sodium pentobarbital (25 mg/kg). Under intratracheal intubation and controlled respiration with a positive-pressure respirator (model SN-480-5; Shinano Seisakusho, Tokyo), a longitudinal cervical incision was made, and both carotid arteries were carefully exposed. The diameters of the carotid arteries were measured *in situ* using a focus eyepiece and a bow compass as previously described.[16] The carotid artery blood flow was then measured as previously described with an electromagnetic flow probe (Nihon Kohden Co., Tokyo).[14,15] The appropriate size of probe was selected for each measurement. The blood flow on the shunt side was measured just proximal to the fistula. Wall shear stress was calculated for the carotid arteries using the Poiseuille formula as previously described.[16] After blood flow measurement, a high-fidelity catheter-tip micromanometer (3F; Millar Instruments Inc., Houston, TX, USA) was introduced into the aortic arch through the right carotid artery. Aortic pressure was recorded in the stable basal state, and the catheter was then advanced into the left ventricle. Hemodynamic data, including blood flow, heart rate, aortic pressure, left ventricular pressure, and its first derivatives were recorded on an eight-channel multipurpose data-acquisition system (MacLab; Analog Digital Instruments Pty Ltd., Sydney, Australia) connected to a Macintosh computer. Hemodynamic variables were digitized at 450 Hz, and stored on a computer for later analysis. The total peripheral resistance index was calculated as mean blood pressure / cardiac index. In this study, the time constant of isovolumic LV pressure relaxation (τ) was calculated from the dp/dt versus pressure relation as previously described.[17,18]

After the hemodynamic recording, the rabbits were killed with an intravenous overdose of pentobarbital. The heart was immediately excised and placed into ice-cold saline to remove the blood. After removal of the atria and large vessels, the ventricles were blotted dry, and the right ventricle was dissected along its *septal insertion*, separated from the rest of the ventricular mass, and weighed. Ventricular myocardial tissue was stored in liquid nitrogen until used.

Northern blot analysis: Northern blot analyses were performed using 15 μg of total RNA as previously described.[15] Probes used in the present study were cDNA fragments encoding α-skeletal actin and β-myosin heavy chain (MHC) (kind gifts from Drs. GJ Babu and M Periasamy of Ohio State University, Columbus, OH). The cDNA fragment encoding the rabbit atrial natriuretic factor (ANF) was obtained by polymerase chain reaction using primers based on a published sequence.[19]

Statistical analysis: Values are expressed as the mean±SE. Comparisons among sham and shunt groups were performed by ANOVA followed by Bonferroni's test. A probability of <0.05 was considered *statistically significant*.

RESULTS

Hemodynamic changes after arterio-venous shunt formation and effects of L-NAME: Cardiac output was increased after arterio-venous shunt formation (Figure 1). Six weeks after the surgery, cardiac output was about 2.2-fold greater

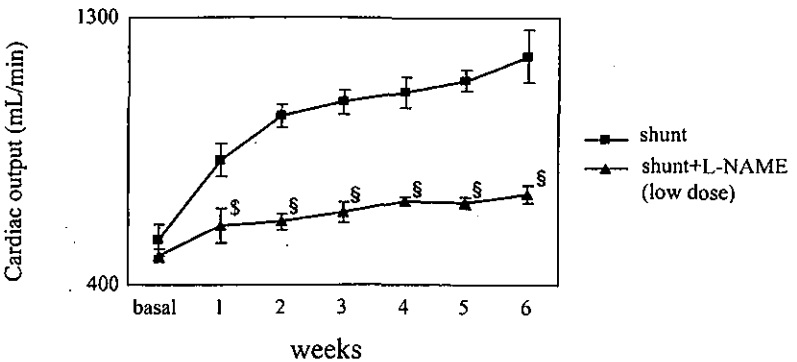

Figure 1. Increment of cardiac output after shunt formation. Chronic treatment with L-NAME attenuated this increase in cardiac output. ‡$P<0.05$ vs shunt

Table I. Body Weight, Heart Rate, and Blood Pressure in Sham, Shunt, and Shunt Rabbits Treated with L-NAME

	Sham (n=8)	Shunt (n=8)	Shunt+L-NAME (low dose) (n=8)	Shunt+L-NAME (high dose) (n=5)
Body weight (kg)	2.99±0.07	2.90±0.03	2.46±0.11†§	2.56±0.10†‡
Heart rate (beats/min)	325±15	331±5	271±7†§	313±16
Systolic blood pressure (mmHg)	126±4	122±4	139±3*§	139±4*§
Diastolic blood pressure (mmHg)	102±2	92±3*	108±3§	105±3§
Mean blood pressure (mmHg)	115±3	107±3	123±3*§	121±2§

Values are expressed as mean±SE. *P<0.05 vs sham, †P<0.01 vs sham, ‡P<0.05 vs shunt, §P<0.01 vs shunt

Table II. Vascular Remodeling of Carotid Artery

	Contra-lateral side (right)		Shunt side (left)	
	Flow (mL/min)	Diameter (mm)	Flow (mL/min)	Diameter (mm)
Sham	31±6	1.88±0.13	46±14	1.90±0.05
Shunt	63±16*	2.30±0.10*	568±67†	4.08±0.29†
Shunt+L-NAME (low dose)	27±5‡	2.02±0.08	325±64†‡	3.40±0.23†‡
Shunt+L-NAME (high dose)	34±3‡	1.75±0.11§	195±14†§	3.06±0.19†§

Values are expressed as mean±SE. *P<0.05 vs sham, †P<0.01 vs sham, ‡P<0.05 vs shunt, §P<0.01 vs shunt

than the basal condition. This increase was significantly attenuated by L-NAME treatment (P<0.05). Six weeks after shunt formation, there was no significant difference in systolic blood pressure between the sham group and shunt group with no treatment (Table I). Chronic L-NAME treatment slightly but significantly elevated blood pressure (P<0.01) compared to the shunt group with no treatment (Table I). Shunt rabbits given L-NAME had a lower mean body weight than shunt rabbits with no treatment (P<0.01).

Vascular remodeling of carotid arteries: Immediately after shunt formation, there was no difference in the blood flow of the carotid artery proximal to the fistula among the shunt groups (data not shown). Six weeks after the shunt formation, the proximal carotid blood artery flow was notably increased (Table II, P<0.01) and dilatation of the flow-loaded artery was evident compared with the sham (P<0.01). These changes were partially but significantly attenuated by L-NAME treatment.

Cardiac morphology and function: Figure 2 illustrates representative tracings of the B-mode and M-mode echocardiograms. In the shunt group, marked cardiac

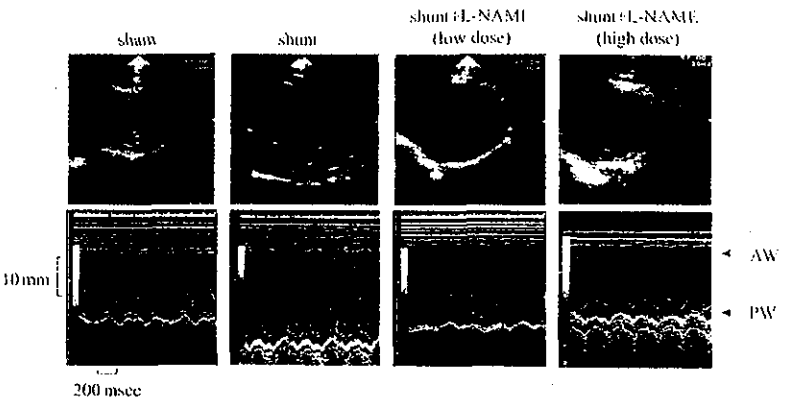

Figure 2. Representative examples of B-mode (top) and M-mode (bottom) echocardiograms in sham, shunt, and shunt treated with L-NAME. In the shunt group, marked left ventricular dilatation was noted. Chronic L-NAME treatment significantly attenuated ventricular dilatation. AW=anterior wall; PW=posterior wall.

Table III. Echocardiography

	Sham (n=8)	Shunt (n=8)	Shunt+L-NAME (low dose) (n=8)	Shunt+L-NAME (high dose) (n=5)
AWTh (mm)	2.25±0.07	2.08±0.09	2.46±0.19	2.38±0.26
PWTh (mm)	2.75±0.17	3.04±0.14	2.87±0.22	2.34±0.18‡
LVDd (mm)	12.96±0.74	17.70±0.68†	14.78±0.42*§	13.38±0.63§
LVDs (mm)	6.86±0.46	11.46±0.50†	9.33±0.34†§	8.40±0.39§
RWT	0.45±0.04	0.28±0.02†	0.36±0.01*	0.34±0.03†
FS (%)	41±2	36±1	37±2	37±1

Values are expressed as mean±SE. AWTh=anterior wall diastolic thickness; PWTh=posterior wall diastolic thickness; LVDd=left ventricular end-diastolic dimension; LVDs=left ventricular end-systolic dimension; RWT=relative wall thickness; FS=fractional shortening. *P<0.05 vs sham, †P<0.01 vs sham, ‡P<0.05 vs shunt, §P<0.01 vs shunt

dilatation (P<0.01) was observed, and the relative wall thickness was significantly decreased (P<0.01) compared to sham, indicating eccentric cardiac hypertrophy (Table III). L-NAME treatment significantly attenuated left ventricular dilatation (P<0.01) and slightly increased relative wall thickness compared to the shunt with no treatment.

Table IV presents the left ventricular hemodynamics. There was no significant difference in heart rate among the groups. In the shunt rabbits, negative dp/dt was significantly increased (P<0.01) and the time constant of LV pressure

Table IV. Left Ventricular Hemodynamics

	Sham (n=8)	Shunt (n=8)	Shunt+L-NAME (low dose) (n=8)
HR (bpm)	300±11	296±8	289±4
LVEDP (mmHg)	-3±1	3±1†	1±1
Peak LVP (mmHg)	131±4	127±4	141±2‡
Max dp/dt (mmHg/sec)	8707±317	8829±742	9501±324
Minimum dp/dt (mmHg/sec)	-9413±604	-6518±549†	-7561±368*
τ (ms)	7±1	10±1†	11±1†

Values are expressed as mean±SE. LVEDP=left ventricular end diastolic pressure; LVP=left ventricular pressure; τ: time constant of left ventricular pressure relaxation. *P<0.05 vs sham, †P<0.01 vs sham, ‡P<0.05 vs shunt.

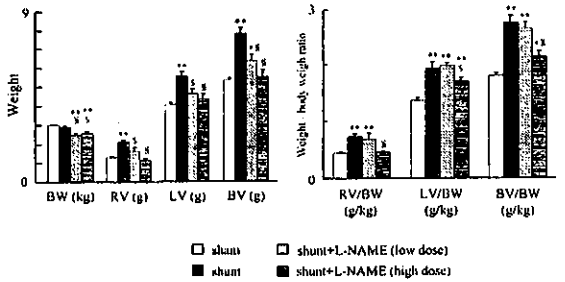

Figure 3. Absolute ventricular weights and ventricular/body weight ratios in the 4 groups. Data are mean±SE. BW, body weight; RV, right ventricle; LV, left ventricle; BV, RV+LV. *P<0.05 vs sham, **P<0.01 vs sham, §P<0.05 vs shunt, ‖P<0.01 vs shunt

decline was prolonged (P<0.01) compared to the sham rabbits, suggesting impaired diastolic function in this volume-overload model. Left ventricular end-diastolic pressure was slightly higher in the shunt group (P<0.01). On the other hand, systolic LV function determined by positive dp/dt was preserved. Chronic inhibition of NO synthesis did not modify the systolic and diastolic function of the left ventricle in this volume-overload model.

Postmortem analysis of cardiac hypertrophy: Right and left ventricular hypertrophy was noted in the shunt rabbits (Figure 3). Significant reductions in right and left ventricular weights were observed in the L-NAME-treated shunt rabbits. The right ventricular weight/body weight, left ventricular/body weight, and biventricular weight/body weight ratios were reduced by treatment with a high dose

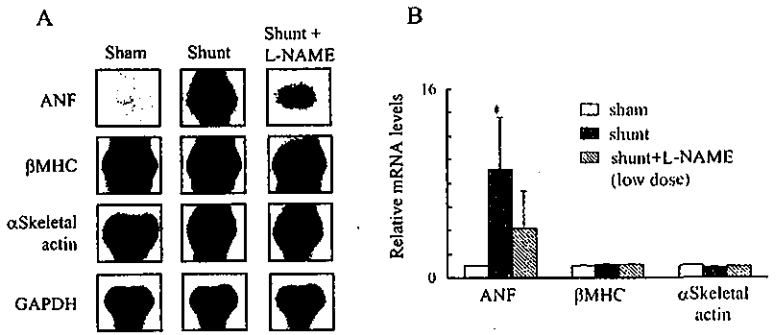

Figure 4. Representative Northern blots (A) and quantitative data by densitometry (B) of hypertrophic gene expressions. Fifteen μg of total RNA was loaded onto each gel lane. GAPDH was used as an internal standard. The mRNA expression of ANF was increased in shunt rabbits, and this up-regulation was attenuated by L-NAME. Data are mean±SE. * P<0.05 vs sham

of L-NAME (P<0.01).

Hypertrophic gene expression by Northern blotting: Figure 4 shows representative Northern blots of hypertrophic genes, such as ANF, β-MHC, and α-skeletal actin. Chronic volume-overload induced the re-expression of ANF. Unexpectedly, the mRNA levels of β-MHC and α-skeletal actin in the left ventricular myocardium were unchanged in this volume-overload-induced cardiac hypertrophy. The recapitulation of ANF in the left ventricular myocardium by volume-overload was partially inhibited by chronic L-NAME treatment.

Discussion

In the present study, we examined the systemic effects of NO inhibition in the progression of eccentric cardiac hypertrophy and vascular remodeling after arteriovenous shunt formation. Left ventricular dilatation, increased cardiac output, and vascular enlargement by shunt formation were attenuated by chronic L-NAME treatment. Increased expression of ANF mRNA in the hypertrophied heart of the shunt rabbits was attenuated by L-NAME.

Flow-induced vascular remodeling was suppressed by L-NAME: As reported in previous studies, we have demonstrated here that NO plays an important role in flow-induced vascular remodeling.[5,16,20] The importance of NO in vascular remodeling has been implicated in disease states such as hypertension, atherosclerosis, and diabetes mellitus, that are associated with endothelial dysfunction.[21,22] A previous study using a genetically engineered mouse has shown that eNOS deficiency did not remodel the carotid artery in response to ligation.[5] The results of the present study are also consistent with a previous report using a rab-

bit model which found that flow-induced vascular remodeling is at least in part NO-dependent.[16] Guzmann, *et al* also reported that flow-induced vascular remodeling is inhibited by the suppression of NO synthesis *in vivo* in rats.[20]

Effects of L-NAME on cardiac function: In this arteriovenous shunt rabbit model, we demonstrated an increase in cardiac output that is consistent with a previous report using an arteriovenous fistula in rats.[23] We showed that this increase in cardiac output was partially attenuated by chronic L-NAME treatment. This finding suggests that the progressive increment of cardiac output after arterio-venous shunt formation is, at least in part, NO dependent. The possible mechanisms by which L-NAME inhibited the increment of cardiac output are as follows; 1) a systemic deficiency of NO that reduces systemic organ blood flow, resulting in decreases in blood supply to the heart, 2) a local deficiency of NO in the flow-loaded artery inhibits flow-induced vascular enlargement, resulting in a decrease in venous return to the heart, and 3) increased after-load by vasoconstriction.

There is now convincing evidence from studies in several different species to support a role for NO in modulating basal myocardial function, particularly relaxation.[24,25] However, these studies investigated only the acute influence of NO on myocyte or myocardial function. To our knowledge, whether or not long term NO deficiency may influence myocardial function has not been rigorously examined. Hypertrophied myocardium is characterized by abnormal relaxation and endothelial dysfunction. Previous reports have suggested that the relaxant effect of NO is impaired in hypertrophied myocardium.[26] Our model of cardiac hypertrophy by volume-overload was accompanied by diastolic dysfunction even in the chronic inhibition of NO synthesis. In this volume-overload model, we reported that diastolic dysfunction was associated with the reduced gene expression of Ca^{2+} cycling proteins.[15]

Effects of NO on cardiac hypertrophy and morphology: NO is reported to have antihypertrophic activity *in vitro* in several cell types, including myocytes.[11-13] Thus, it would be expected that chronic inhibition of NO synthesis induces cardiac hypertrophy *in vivo*. However, the results regarding cardiac hypertrophy from L-NAME-treated animals are controversial.[6-8,27,28] These contradictory results may be related to the doses of L-NAME used and the duration of treatment. One study, which used a low dose of L-NAME (7.5 mg/kg/day) for 2, 4, and 6 months, reported a significant reduction in the left ventricular index in L-NAME-treated rats in spite of hypertension.[27] However, the role of NO *in vivo* in cardiac hypertrophy is still unclear because it is difficult to assess the growth inhibitory effect of NO independently from changes in cardiac loading conditions. In the present study, chronic L-NAME treatment reduced the ventricular weight/body weight ratio in shunt rabbits, although blood pressure was slightly

increased by L-NAME. L-NAME also reduced left ventricular chamber size and inhibited the up-regulation of ANF genes by volume-overload. These data suggest that chronic inhibition of NO production by L-NAME may have an antihypertrophic effect, at least in part, in this animal model of eccentric hypertrophy by volume-overload.

Conclusion: The present study emphasizes the importance of NO in blood flow regulation and vascular remodeling. NO is involved in the increase in cardiac output after arteriovenous shunt formation. NO systemically controls the mechanical loading conditions to the heart by changing blood pressure and regional blood flow. We conclude that in this arteriovenous shunt model, NO plays a pivotal role in the progression of cardiovascular remodeling by regulating the loading conditions of the heart.

REFERENCES

1. Tomoike H. Responses of the heart to mechanical stress. In: Hayashi K, Kamiya A, Ono K, editor. *Biomechanics: Functional Adaptation and Remodeling*. Tokyo: Springer-Verlag 1996: 59-75.
2. Gibbons GH, Dzau VJ. The emerging concept of vascular remodeling. N Engl J Med 1994; 330: 1431-8.
3. Kuchan MJ, Frangos JA. Role of calcium and calmodulin in flow-induced nitric oxide production in endothelial cells. Am J Physiol 1994; 266: C628-36.
4. Awolesi MA, Sessa WC, Sumpio BE. Cyclic strain upregulates nitric oxide synthase in cultured bovine aortic endothelial cells. J Clin Invest 1995; 96: 1449- 54.
5. Rudic DR, Shesely GE. Direct evidence for the importance of endothelium-derived nitric oxide in vascular remodeling. J Clin Invest 1998; 101: 731-6.
6. Numaguchi K, Egashira K, Takemoto M, *et al*. Chronic inhibition of nitric oxide synthesis causes coronary microvascular remodeling in rats. Hypertension 1995; 26: 957-62.
7. Devlin AM, Brosnan MJ, Graham D, *et al*. Vascular smooth muscle cell polyploidy and cardiomyocyte hypertrophy due to chronic NOS inhibition *in vivo*. Am J Physiol 1998; 274: H52-9.
8. Kobayashi N, Hara K, Watanabe S, Higashi T, Matsuoka H. Effect of imidapril on myocardial remodeling in L-NAME-induced hypertensive rats is associated with gene expression of NOS and ACE mRNA. Am J Hypertens 2000; 13: 199-207.
9. Takemoto M, Egashira K, Usui M, *et al*. Important role of tissue angiotensin- converting enzyme activity in the pathogenesis of coronary vascular and myocardial structural changes induced by long-term blockade of nitric oxide synthesis in rats. J Clin Invest 1997; 99: 278-87.
10. de Oliveira CF, Nathan LP, Metze K, *et al*. Effect of Ca^{2+} channel blockers on arterial hypertension and heart ischaemic lesions induced by chronic inhibition of nitric oxide synthesis in the rat. Eur J Pharmacol 1999; 373: 195-200.
11. Kolpakov V, Kulik TJ. Nitric oxide-generating compounds inhibit total protein and collagen synthesis in cultured vascular smooth muscle cells. Circ Res 1995; 76: 305-9.
12. Ritchie RH, Schiebinger RJ, LaPointe MC, Marsh JD. Angiotensin II-induced hypertrophy of adult rat cardiomyocytes is blocked by nitric oxide. Am J Physiol 1998; 275: H1370-4.
13. Ishigai Y, Mori T, Ikeda T, Fukuzawa A, Shibano T. Role of bradykinin-NO pathway in prevention of cardiac hypertrophy by ACE inhibitor in rat cardiomyocyte. Am J Physiol 1997; 273: H2659-63.
14. Tojo T, Tsunoda Y, Nakada S, Tomoike H. Effects of long-term treatment with nonselective endothelin receptor antagonist, TAK-044, on remodeling of cardiovascular system with sustained volume overload. J Cardiovasc Pharmacol 2000; 35: 777-85.

15. Takahashi N, Atsumi H, Nakada S, Takeishi Y, Tomoike H. Alterations in the inotropic responses to forskolin and Ca^{2+} and reduced gene expression of Ca^{2+}-signaling proteins induced by chronic volume overload in rabbits. Jpn Circ J 2000; 64:861-7.
16. Tronc F, Wassef M, Esposito B, Henrion D, Glagov S, Tedgui A. Role of nitric oxide in flow-induced remodeling of the rabbit common carotid artery. Arterioscler Thromb Vasc Biol 1996; 16: 1256-62.
17. Raff GL, Glantz SA. Volume loading slows left ventricular isovolumic relaxation rate. Circ Res 1981; 48: 813-24.
18. Gilbert JC, Glantz SA. Determinants of left ventricular filling and of the diastolic pressure-volume relation. Circ Res 1989; 64: 827-52.
19. Oikawa S, Imai M, Inuzuka C, Tawamgi Y, Nakazato H, Matsuo H. Structure of dog and rabbit precursors of atrial natriuretic polypeptides. Deduced from nucleotide sequence of cloned cDNA. Biochem Biophys Res Commun 1985; 132: 892-9.
20. Guzman RJ, Abe K, Zarins CK. Flow-induced arterial enlargement is inhibited by suppression of nitric oxide synthase activity *in vivo*. Surgery 1997; 122: 273-80.
21. Rudic RD, Sessa WC. Nitric oxide in endothelial dysfunction and vascular remodeling: clinical correlates and experimental links. Am J Hum Genet 1999; 64: 673-7.
22. Gibbons GH. Endothelial function as a determinant of vascular function and structure: a new therapeutic target. Am J Cardiol 1997; 79: 3-8.
23. Huang M, Hester RL, Guyton AC. Hemodynamic changes in rats after opening an arteriovenous fistula. Am J Physiol 1992; 262: H846-51.
24. Shah AM. Paracrine modulation of heart cell function by endothelial cells. Cardiovasc Res 1996; 31: 847-67.
25. Paulus WJ, Shah AM. NO and cardiac diastolic function. Cardiovasc Res 1999; 43: 595-606.
26. MacCarthy PA, Shah AM. Impaired endotheluim-dependent regulation of ventricular relaxation in pressure-overload cardiac hypertrophy. Circulation 2000; 101: 1854-60.
27. de Oliveira CF, Cintra KA, Teixeira SA, De Luca IM, Antunes E, De Nucci G. Development of cardiomyocyte hypertrophy in rats under prolonged treatment with a low dose of a nitric oxide synthesis inhibitor. Eur J Pharmacol 2000; 391: 121-6.
28. Amal JF, Amrani AI, Chatellier G, Menard J, Michel JB. Cardiac weight in hypertension induced by nitric oxide synthase blockade. Hypertension 1993; 22: 380-7.

Impaired Pulmonary Inflammatory Responses Are a Prominent Feature of Streptococcal Pneumonia in Mice with Experimental Emphysema

Sumito Inoue, Hidenori Nakamura, Kazuhisa Otake, Hiroshi Saito, Kyoko Terashita, Jun Sato, Hiroaki Takeda, and Hitonobu Tomoike

First Department of Internal Medicine, Yamagata University School of Medicine, Yamagata; Respiratory Medicine, Sei-rei Hamamatsu General Hospital, Shizuoka, Japan

Little is known about why patients with chronic obstructive pulmonary disease are susceptible to bacterial infections. Using an animal model of pulmonary emphysema, we investigated the inflammatory responses to bacterial infection. After intratracheal infection with *Streptococcus pneumoniae* (10^3–10^7 cfu/mouse), the control mice did not die. However, the mice with emphysema died in a dose-dependent manner. Bronchoalveolar lavage fluid, examined 24 hours after infection showed that the numbers of total cells and neutrophils, in addition to murine tumor necrosis factor-α and macrophage inflammatory protein-2 concentrations, were significantly less in the mice with emphysema compared with the control mice. Histopathologic findings revealed that the alveoli were filled with inflammatory cells and exudate in the control mice but not in the mice with emphysema. Seventy-two hours after infection, serum cytokine levels were significantly higher in the mice with emphysema, and significant numbers of *S. pneumoniae* were detected in both the whole lung tissues and the blood of mice with emphysema. These findings suggest that the inflammatory response in mice with emphysema was impaired at the site of bacterial infection despite the bacteremia, which accelerated severe systemic inflammatory responses. Accordingly, intra-alveolar but not systemic immune responses to bacterial infection were impaired in the presence of experimental emphysema.

Keywords: chronic obstructive pulmonary disease; bacterial infection; cytokine; *Streptococcus pneumoniae*; bacteremia

Chronic obstructive pulmonary disease (COPD) is a common disease, characterized by various levels of airflow obstruction, and it is one of the major medical problems in developed countries, including Japan (1–6). The natural history of COPD is associated with frequent respiratory tract infections, which result in exacerbation, severe respiratory failure, and death (7–9). Recurrent infection of the respiratory tract leads to significant problems for patients with COPD not only by way of medical complications but also by way of costs of care (4, 5, 10–14).

COPD is generally considered to be an important predisposing condition for pneumonia, although conclusive or definitive evidence showing that the risk of pneumonia for patients with COPD is higher than for the general population remains to be confirmed (15–17). Specifically, little is known about the precise mechanisms of how or why patients with COPD are susceptible to bacterial infection. In addition, there have been few studies about bacterial infection of the respiratory tracts in animal models of COPD. The purpose of the present study was to investigate the pathophysiology of the susceptibility to bacterial infection in patients with COPD, using a mouse model of elastase-induced pulmonary emphysema. Because *Streptococcus pneumoniae* is one of the major bacterial pathogens of respiratory infections in patients with COPD (4, 7, 8, 12, 18), we used it as a pathogen.

METHODS

Animals

Specific pathogen-free male ICR mice, 8 weeks of age, were purchased from Japan Clea Co. (Tokyo, Japan). All experiments using mice in this study were approved by the institutional animal care and use committee.

Preparation of *S. pneumoniae*

S. pneumoniae Serotype 3 (Otsuka Pharmaceutical Co. Ltd., Tokushima, Japan) is penicillin-sensitive. The minimal inhibitory concentration of penicillin G against the organism was less than or equal to 0.06 μg/ml. *S. pneumoniae* were incubated at 37°C in tryptic soy broth (DIFCO, Detroit, MI) with 10% fetal bovine serum. The bacterial number was estimated by measuring the optical density at 660 nm with a spectrophotometer. The challenged bacterial number was determined by counting by the number of colonies on the blood agar plates (19–23).

An Emphysematous Model

To produce pulmonary emphysema, mice were anesthetized with an intraperitoneal injection of thiopental sodium (150 mg/kg body weight), and the trachea was intubated with a 22-gauge cannula. Porcine pancreatic elastase (PPE) (Calbiochem-Novabiochem Co., USA) in phosphate-buffered salt solution (PBS) was intratracheally administered via a cannula in doses of 6 (n = 5), 9 (n = 5), 12 (n = 5) unit/50 μl. Control mice (n = 5) were treated similarly but with 50 μl of PBS (24–29).

Streptococcal Infection

Three weeks after 12 U of elastase treatment, suspensions containing 10^3 to 10^7 cfu of *S. pneumoniae*/100 μl broth were intratracheally administered to both control (n = 52) and mice with emphysema (n = 63) under conditions of intraperitoneal anesthesia.

Preparation of Serum

At 24 and 72 hours after inoculation, whole blood was obtained by direct puncture of the right ventricular cavity in mice, which had been deeply anesthetized with excess intraperitoneal thiopental sodium (450 mg/kg body weight). Individual sera were separated from the clotted blood by centrifugation and stored at −80°C until the assays were performed.

Bronchoalveolar Lavage

After blood was drawn by direct puncture of the right ventricle, bronchoalveolar lavage (BAL) was performed. In brief, a 22-gauge cannula was wedged into the trachea. Three milliliters of PBS was infused and recovered via a cannula. These manipulations were performed gently

(Received in original form May 23, 2001; accepted in final form December 2, 2002)

Supported by grants-in-aid for scientific research (10307016, 11557044) from the Ministry of Education, Science, Sports and Culture, Japan.

Correspondence and requests for reprints should be addressed to Sumito Inoue, M.D., First Department of Internal Medicine, Yamagata University School of Medicine, 2-2-2, Iida-Nishi, Yamagata 990-9585, Japan. E-mail: BYC04033@nifty.ne.jp

Am J Respir Crit Care Med Vol 167. pp 764–770, 2003
DOI: 10.1164/rccm.2105111
Internet address: www.atsjournals.org

to avoid artificial lung injury. Cytologic preparations were made using centrifugation (Cytospin 2; Shandon, Pittsburgh, PA) and were stained with modified May-Giemsa stain (Diff Quick; American Science Products, McGaw Park, IL). Differential cell counts were performed on 200 cells per sample. Cells were removed from BAL fluids (BALF) by centrifugation at 200 × *g* for 10 minutes, and supernatants of BALF were stored at −80°C until evaluation.

Biochemical Analysis of BALF and Serum

Murine tumor necrosis factor-α (TNF-α), KC (cytokine-induced neutrophil chemoattractant, CXCL1), and macrophage inflammatory protein-2 (MIP-2) in both BALF and serum were measured by ELISA (Quantikine; R&D Systems, Minneapolis, MN) because these cytokines are known to act as key molecules in inflammatory responses in bacterial infections (30–37).

Histologic Analysis

For morphologic examinations, both lungs were inflated under constant positive pressure at 25 cm water pressure with 10% buffered formaldehyde and were then perfuse-fixed. The fixed lungs were embedded in paraffin, stained with hematoxylin and eosin, and examined using a microscope (BX50F4; Olympus, Tokyo, Japan) (38). The severity of structural alternations in the emphysematous model was determined morphometrically using the mean linear intercept of the airspaces. This is one of the more common parameters for determining emphysema in laboratory animals and humans (25, 28, 39, 40). We evaluated 10 randomly selected fields per lobe or lung part. The whole lung mean linear intercept value was derived as a mean of the left and right lung mean linear intercept values.

Bacteriologic Examination

The severity of bacterial infection in the lung tissue and blood were quantitatively evaluated as bacterial colony numbers after infection. Namely, lungs were homogenized in 1 ml of PBS, and the homogenates were serially diluted 10-fold with PBS. One hundred microliters of the diluents of lung homogenates or 10 μl of blood were spread on blood agar plates. The plates were incubated at 37°C with 5% carbon dioxide for 18 hours (22, 41). The bacterial numbers were determined by counting the colonies on the plates, and expressed as cfus.

Statistical Analysis

All values are expressed as means ± SEM. Two-factor functional analysis of variance was performed to assess differences between the groups. The differences between the groups or between periods were further compared using Tukey-Kramer tests with an adjustment of the p values ($p < 0.05$). A p value of less than 0.05 was considered statistically significant.

RESULTS

Severity of Experimental Pulmonary Emphysema

After intratracheal elastase instillations, we confirmed histologically the dose-dependent emphysematous changes throughout the lung (data not shown). Morphometric analyses demonstrated that the mean linear intercept in lungs from elastase-treated mice were significantly increased in a dose-dependent manner (control mice; 33.90 ± 0.68 μm, PPE 6 U; 41.98 ± 1.66 μm, PPE 9 U; 50.31 ± 1.06 μm, PPE 12 U; 67.21 ± 2.00 μm, $p < 0.05$, control vs. PPE 6 U, 9 U, and 12 U, PPE 6 U vs. PPE 9 U, and 12 U, PPE 9 U vs. PPE 12 U). In the following experiments, we used 12 U of PPE to produce experimental emphysema.

Survival After Infection

Figure 1 illustrates the survival curves obtained from four groups of mice with different doses of *S. pneumoniae* inoculation. The control mice did not die after a challenge of *S. pneumoniae* up to a dose of 4.9×10^7 cfu/mouse. Mice with emphysema became emaciated and died in a dose-dependent manner within several days. Mice with emphysema without infection survived throughout the observation period.

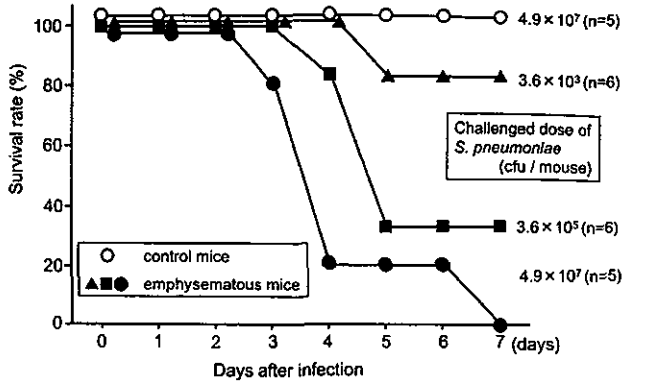

Figure 1. Survival rate in control and mice with emphysema. Control mice did not die after challenge with 4.9×10^7 cfu/mouse of *S. pneumoniae*. Mice with emphysema died after challenge with $3.6 \times 10^3 \sim 4.9 \times 10^7$ cfu/mouse of *S. pneumoniae* in a challenged bacterial dose-dependent fashion.

BALF Analysis

Cell numbers and differential cell counts. Cell compositions of BALF are summarized in Figure 2. There was no significant difference in the volume of the lavage fluid retrieved between the two groups of mice (control mice 2.46 ± 0.64 ml vs. mice with emphysema 2.26 ± 0.55 ml; not significant). Before infection, there were no significant differences in total cell counts and cellular profiles between the control and mice with emphysema. At 24 hours after infection, total cell counts, especially neutrophils, were significantly increased in the control mice. The number of total cells and neutrophils in BALF from the mice with emphysema were significantly lower than those of the control mice. Seventy-two hours after infection, there were no significant differences in cellular counts between the control and mice with emphysema.

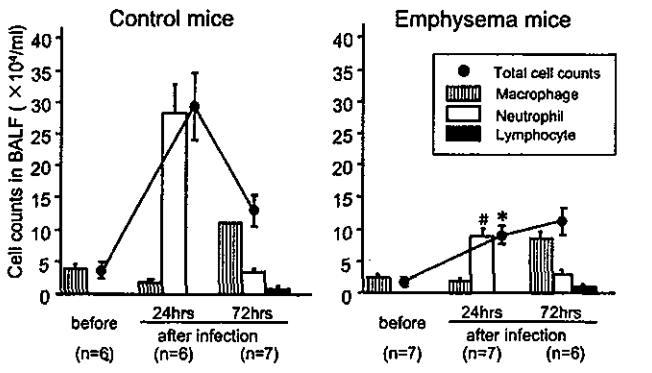

Figure 2. Total cell counts and differential cell counts in BALF. Before infection, there were no significant differences in total cell counts and cellular profiles between control and mice with emphysema. At 22 hours after infection, total cell counts, especially neutrophils, were significantly increased in control mice ($p < 0.05$). The numbers of total cells and neutrophils in BALF from mice with emphysema were significantly lower than those of control mice. A total of 4.9×10^7 cfu/mouse of *S. pneumoniae* were challenged. #p value less than 0.05 compared with the neutrophil counts in control mice at 24 hours. *p value less than 0.05 compared with the total cell counts in control mice at 24 hours.

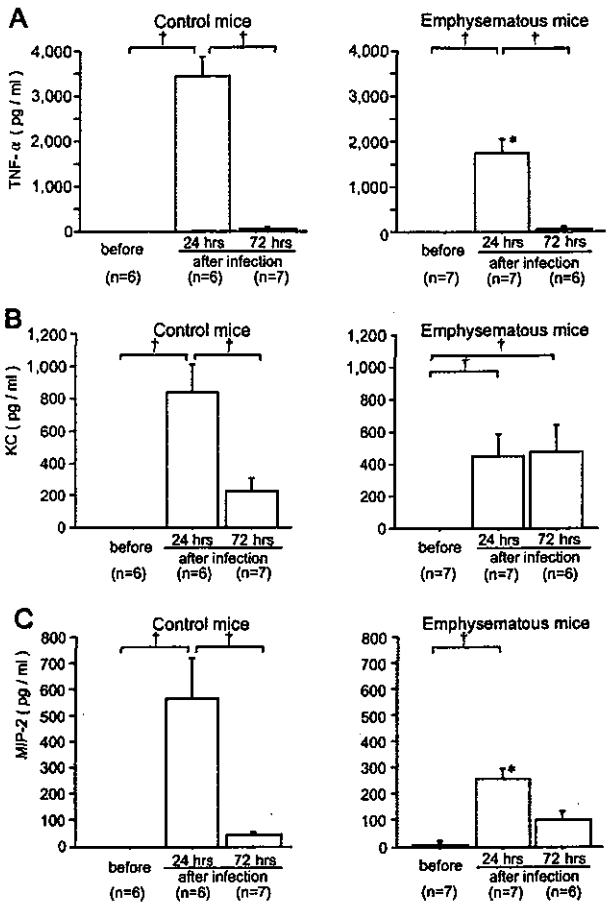

Figure 3. Time course of TNF-α (A), KC (B), and MIP-2 (C) levels in BALF from control and mice with emphysema. TNF-α and MIP-2 levels in mice with emphysema were significantly lower than in control mice 24 hours after infection. Seventy two hours after infection, TNF-α levels in control and mice with emphysema, and KC and MIP-2 levels in control mice significantly decreased compared with those at 24 hours after infection. A total of 4.9×10^7 cfu/mouse of *S. pneumoniae* were challenged. † p value less than 0.05. *p value less than 0.05 compared with control mice. MIP-2, macrophage inflammatory protein-2; TNF-α, tumor necrosis factor-α.

Cytokine levels in BALF. Time course of the levels of TNF-α, KC, and MIP-2 in BALF after infection are shown in Figures 3A–3C. Before infection, the levels of these cytokines in BALF were very low in both the control and mice with emphysema. At 24 hours after infection, TNF-α, KC, and MIP-2 levels in the control mice were significantly increased, however, the extent of TNF-α and MIP-2 increases in the mice with emphysema were significantly lower than in the control mice.

At 72 hours, TNF-α, KC, and MIP-2 levels in BALF decreased from the 24-hour level in the control mice. In the mice with emphysema, the cytokines levels decreased except for KC.

Histologic Changes After Infection

Representative microscopic findings of the lungs in the control and mice with emphysema 24 and 72 hours after infection are shown in Figure 4. In the control mice, the alveoli were filled with inflammatory cells, especially neutrophils and exudate, 24 hours after infection (Figure 4A), and the inflammatory cells and exudate disappeared from the alveolar spaces 72 hours after infection (Figure 4B). In the mice with emphysema, inflammatory cell infiltrations in alveolar spaces were less at both 24 and 72 hours after infection (Figures 4C and 4D). Alveolar wall thickening with eosinophilic materials and capillary congestion with red blood cells were evident in the mice with emphysema at 72 hours.

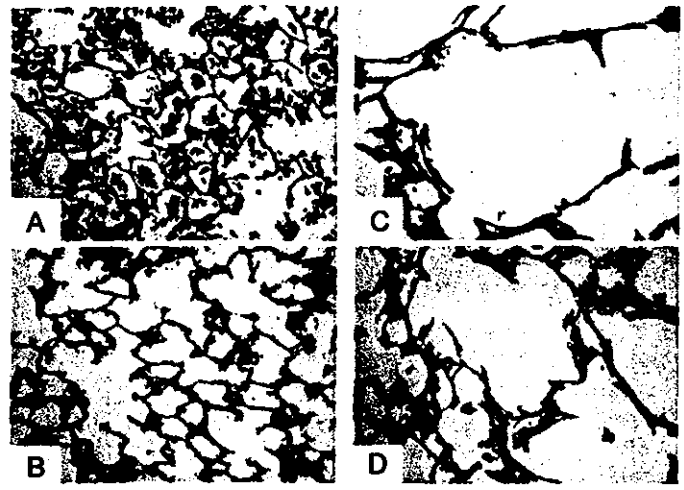

Figure 4. Histologic findings of the lung tissue sections (hematoxylin and eosin stain, ×200). A total of 4.9×10^7 cfu/mouse of *S. pneumoniae* were challenged. (A) Control mice, 24 hours after infection. The alveoli were filled with inflammatory cells, especially neutrophils and exudate. (B) Control mice, 72 hours after infection. Inflammatory cells and exudate disappeared from the alveolar spaces. (C) Mice with emphysema, 24 hours after infection. There were less inflammatory changes in alveolar spaces compared with control mice. Inflammatory cells infiltrated normal-looking alveoli rather than emphysematous alveoli. (D) Mice with emphysema, 72 hours after infection. Alveolar wall thickening with eosinophilic materials and capillary congestion with red blood cells is evident.

Systemic Inflammatory Changes

Before infection, there was no significant difference in white blood cell (WBC) counts in punctured blood between the control and mice with emphysema (Figure 5). At 24 hours after infection,

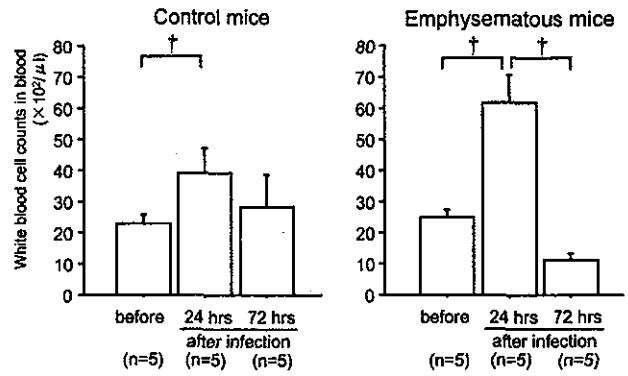

Figure 5. Time course of WBC counts in blood from control and mice with emphysema. At 24 hours after infection, WBC counts in control and mice with emphysema significantly increased compared with WBC counts before infection. At 72 hours, WBC counts decreased in both control and mice with emphysema. Specifically, WBC counts in mice with emphysema tended to decrease below the levels before infection. A total of 1.76×10^5 cfu/mouse of *S. pneumoniae* were challenged. †p value less than 0.05. WBC, white blood cell.

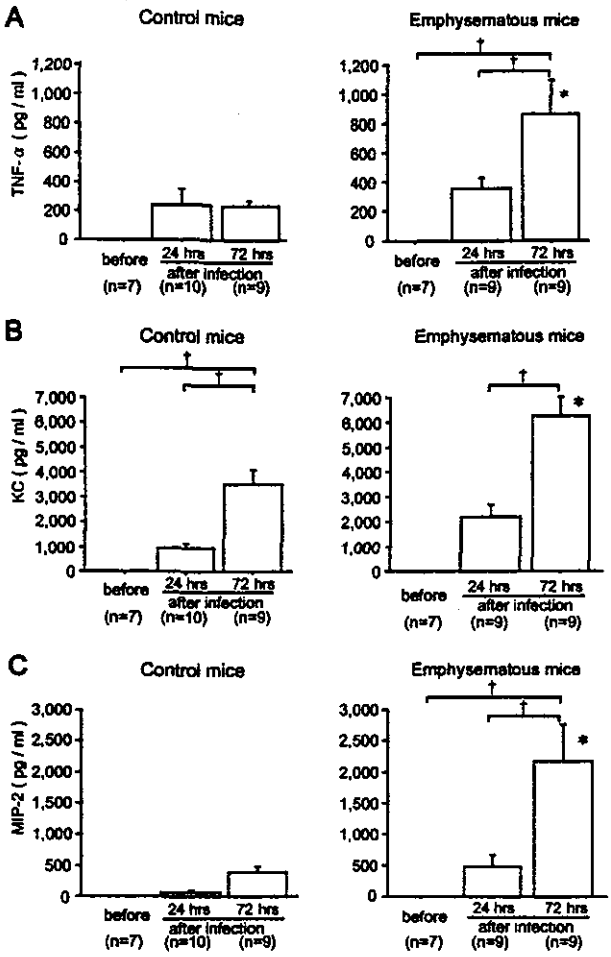

Figure 6. Time course of TNF-α (A), KC (B), and MIP-2 (C) levels in serum from control and mice with emphysema. At 24 hours after infection, each cytokine level in mice with emphysema tended to be higher than those in control mice. TNF-α, KC, and MIP-2 levels 72 hours after infection in mice with emphysema were significantly higher than those in control mice. A total of 4.9×10^7 cfu/mouse of *S. pneumoniae* were challenged. †p value less than 0.05. *p value less than 0.05 compared with control mice. MIP-2, macrophage inflammatory protein-2; TNF-α, tumor necrosis factor-α.

WBC counts in both the control and mice with emphysema were significantly higher than before infection. At 72 hours, WBC counts decreased in both the control and mice with emphysema. Specifically, WBC counts in mice with emphysema tended to decrease after infection.

Serum TNF-α, KC, and MIP-2 levels are summarized in Figures 6A–6C. Before infection, there were no significant differences in TNF-α, KC, and MIP-2 levels between the control and mice with emphysema. After infection, serum cytokine levels increased in both groups of mice 72 hours after infection. Increased levels of serum cytokines were significantly higher in mice with emphysema compared with the control mice.

Bacterial Colony Counts in Whole Lung Tissues and Blood

Bacterial colony numbers from lung tissues are shown in Figure 7. At 24 hours after infection, the bacterial counts in whole lung tissues were not significantly different between the two groups of mice. At 72 hours, the bacterial counts in lung tissues from the control mice decreased. In contrast, the number of bacterial colonies in lung tissues from mice with emphysema

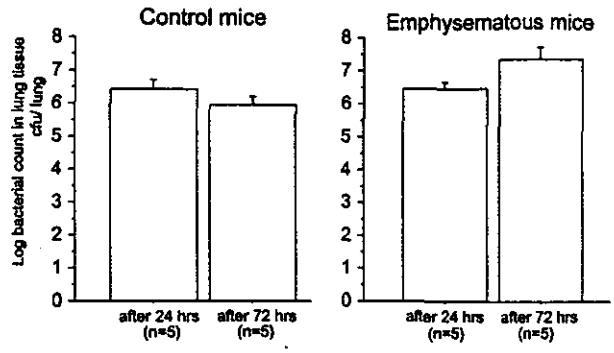

Figure 7. Bacterial counts from total lung tissue after streptococcal infection (log scale). Seventy-two hours after infection, bacterial counts in control mice decreased. In contrast, bacterial colony growth in mice with emphysema markedly increased. A total of 1.76×10^5 cfu/mouse of *S. pneumoniae* were challenged.

markedly increased (control mice $1.71 \pm 0.92 \times 10^6$ cfu/lung, emphysema $7.58 \pm 5.73 \times 10^7$ cfu/lung, NS.).

Bacterial cultures from punctured blood are summarized in Table 1. In two to three of the five control mice, blood cultures were positive for *S. pneumoniae* 24 hours after infection. Quantitatively, the bacterial number had decreased 72 hours after infection in the control mice. In contrast, all mice with emphysema were bacteremic 24 hours after infection, and the numbers of bacteria in blood increased markedly 72 hours after infection.

DISCUSSION

In the present study, we demonstrated the unique inflammatory responses to bacterial infection in the lungs of mice with elastase-induced emphysema. Early responses in the lungs after infection, including the infiltration of neutrophils and production of inflammatory cytokines such as TNF-α or MIP-2, were significantly less in mice with emphysema. These findings are in parallel with the histologic findings. Because inflammatory responses in lungs, such as neutrophil migration and cytokine production, play an important role in host defense in the alveolar space during the acute phase of bacterial infection (30–36, 42), an impaired inflammatory response in the lungs may be one of the most important contributing factors to the susceptibility of infection in mice with experimental emphysema.

Mechanism of the Blunted Inflammatory Response in Lungs of Mice with Emphysema

No clear answer was found to explain why mice with emphysema showed impaired inflammatory responses in lungs. First, the bacteria entering the alveolus are likely to be thrust up against the alveolar wall, where they will become immersed in the epithelial lining fluid. There they would be coated with various nonimmune opsonins and a specific IgG antibody (43, 44). The antibody creates an antigen–antibody reaction that activates a complement sequence resulting in bacterial lysis. A mixture of opsonins adhere to the bacterium and facilitate ingestion by alveolar macrophages. Because the principal function of innate immunity is to rapidly clear inhaled substances to prevent the establishment of an inflammatory process, further studies are needed to clarify whether innate immunity is suppressed in emphysematous lungs.

A second possibility is that alveolar macrophages in emphysematous lungs come into less contact with microbes in the enlarged airspaces *in vivo*. Experimentally, when a bacterial inoculum is instilled onto the alveolar surface, bacteria remain free for